NASA TECHNICAL NOTE

NASA TN D-5377

C. 1

NASA TN D-5377

EXPERIMENTAL AND THEORETICAL TURBULENT BOUNDARY LAYER DEVELOPMENT IN A MACH 4.4 WATER-COOLED CONICAL NOZZLE

by Donald R. Boldman, James F. Schmidt, and Robert C. Ehlers

Lewis Research Center
Cleveland, Ohio

NATIONAL AERONAUTICS AND SPACE ADMINISTRATION • WASHINGTON, D. C. • AUGUST 1969

EXPERIMENTAL AND THEORETICAL TURBULENT BOUNDARY LAYER DEVELOPMENT IN A MACH 4.4 WATER-COOLED CONICAL NOZZLE

By Donald R. Boldman, James F. Schmidt, and Robert C. Ehlers

Lewis Research Center
Cleveland, Ohio

NATIONAL AERONAUTICS AND SPACE ADMINISTRATION

For sale by the Clearinghouse for Federal Scientific and Technical Information
Springfield, Virginia 22151 – CFSTI price $3.00

ABSTRACT

Boundary layer temperature and velocity measurements were obtained at three stations in the supersonic portion of a 30^{o}-15^{o} C-D cooled nozzle operating with an adiabatic and a cooled inlet. Tests were performed with heated air at nominal Mach numbers of 2.1 to 4.4. The ratio of wall-to-stagnation temperature was 0.8 at Mach 2.1 and 0.6 at Mach 4.4. The results indicated that the thermal boundary layer in supersonic flow was not described by a 1/7-power law. The experimental momentum and displacement thicknesses compared favorably to predictions based on the integral boundary layer theories of Bartz and Sasman-Cresci.

EXPERIMENTAL AND THEORETICAL TURBULENT BOUNDARY LAYER DEVELOPMENT IN A MACH 4.4 WATER-COOLED CONICAL NOZZLE

by Donald R. Boldman, James F. Schmidt, and Robert C. Ehlers
Lewis Research Center

SUMMARY

Boundary layer surveys were obtained in the supersonic portion of a 30° half-angle of convergence by 15° half-angle of divergence cooled nozzle operating with heated air. Tests were made with an adiabatic and a cooled inlet in order to alter the thickness of the thermal boundary layer at the nozzle entrance.

The experimental results indicated that the 1/7-power law for a turbulent boundary layer did not describe the thermal boundary layer in the supersonic part of the nozzle. This power law described the velocity profile only when the thermal boundary layer thickness was comparable to the thickness in which the Mach number became constant.

Predictions of the downstream experimental values of momentum thickness by the Bartz and Sasman-Cresci theories were within 18 percent of an experimental uncertainty band imposed by different methods of terminating the integration of the experimental profiles. The Bartz theory accounted for the experimentally observed changes in momentum thickness which accompanied the change in inlet cooling. Predictions from the Sasman-Cresci theory did not reveal any differences in momentum thickness with the different inlet thermal boundary layers.

The Bartz theory tended to underpredict the experimental values of displacement thickness whereas the Sasman-Cresci method overpredicted the data. The amounts of underprediction and overprediction at the downstream survey station were about 16 and 25 percent, respectively.

INTRODUCTION

Optimization of the performance of certain propulsion and wind tunnel nozzles requires an accurate assessment of the turbulent boundary layer. Most conventional

analyses of turbulent boundary layers in accelerated supersonic flows utilize empiricisms derived from studies with nearly zero acceleration. However, various analyses yield widely divergent predictions of the turbulent boundary layer development in supersonic nozzle flows, especially if these flows involve heat transfer. In reference 1, it was suggested that a principal shortcoming of current theories concerns the description of the boundary layer temperature distribution near the nozzle wall. The present study was conducted in order (1) to obtain a better understanding of the complex boundary layer development in supersonic nozzles with heat transfer and (2) to supplement the rather meager inventory of available experimental results dealing with the effects of thermal boundary layer history on the deficiency thicknesses of momentum and displacement in supersonic nozzle flows.

The conical nozzle of this investigation was used previously for gas-side heat transfer experiments which were reported in references 2 to 5. The results of reference 3 revealed that extreme differences in the velocity boundary layer thickness at the nozzle entrance produced a negligible difference in throat heat transfer. Conversely, differences in the thickness of the thermal boundary layer at the nozzle entrance resulted in different throat heat transfer rates (as noted by comparison of the results in refs. 4 and 5). In the current investigation, attention will be devoted to the effects of these different nozzle entrance thermal boundary layer thicknesses on the boundary layer development in the supersonic flow.

Boundary layer velocity and temperature surveys were obtained at three stations in a 30°-15° C-D nozzle. These stations had nominal flow Mach numbers of 2.1, 3.7, and 4.4. All tests were performed with a cooled nozzle wall and back pressure which was sufficient to prevent shock-induced separation. The nominal stagnation temperature and pressure were 970° R (539 K) and 300 pounds per square inch (207 N/cm^2) absolute, respectively. The Reynolds number based on diameter was about 5.5×10^6 and 3.5×10^6 at the upstream and downstream stations, respectively. The ratio of nozzle wall-to-stagnation temperature, which was essentially independent of the inlet cooling, was about 0.8 at the upstream supersonic station and about 0.6 at the downstream station. In order to examine the effects of inlet thermal boundary layer growth on the profiles in the supersonic end of the nozzle, the tests were performed with an adiabatic (uncooled wall) and cooled inlet coupled to the nozzle.

The experimental displacement and momentum thicknesses at the three stations will be compared to theoretical results based on the Bartz analysis (ref. 6) as well as the Sasman-Cresci analysis of reference 7. These integral methods were selected because they typically illustrate some of the differences that can arise in the predicted deficiency thicknesses. The Sasman-Cresci method (ref. 7) involves the simultaneous solution of the momentum and moment of momentum equations whereas the Bartz method (ref. 6) is based on the simultaneous solution of the momentum and energy equations. The skin friction laws and other auxiliary equations in the two methods also differ. Of particular

interest in the supersonic flow field is the power-law assumption for the profiles. The experimental velocity and temperature profiles will be compared to 1/7-power profiles which were assumed in the Bartz analysis (ref. 6).

SYMBOLS

c_f skin-friction coefficient

d local diameter of nozzle

M local Mach number

n interaction exponent

P pressure

$\overline{R}$ gas constant

T temperature

u velocity

x axial distance from nozzle geometric throat

y distance from nozzle wall

z axial distance from nozzle entrance

δ velocity boundary layer thickness

δ^* displacement thickness

Δ temperature boundary layer thickness

γ ratio of specific heats ($\gamma = 1.4$)

θ momentum thickness

φ energy thickness

ρ density

ζ upper limit of integration over boundary layer

Subscripts:

ad adiabatic wall condition

e edge of boundary layer

M based on Mach number

r recovery value

ref reference condition used in temperature recovery ratio calculations

s static condition

t local stagnation condition

t-1 conditions upstream of normal shock

t-2 conditions downstream of normal shock

w wall condition

0 free-stream stagnation condition

∞ free-stream condition

Superscript:

* geometric throat condition

APPARATUS

Facility

The tests were performed in a heated air facility, described in reference 2. This facility, which is shown in figure 1, comprises a heat exchanger, plenum, cylindrical inlet, and test nozzle. The boundary layer in the plenum is removed at the entrance plane of the cylindrical inlet by means of a bypass bleed manifold and flow controller.

Cylindrical Inlets

Two cylindrical inlets were employed in the tests. Both of the inlets had inside diameters of 6.5 inches (16.5 cm) which provided a nozzle contraction area ratio of 19.0 (ratio of inlet to nozzle throat area). One of the inlets operated with an adiabatic (uncooled) wall whereas the other inlet had a water-cooled wall. Details concerning the design of the adiabatic inlets can be obtained from references 2 to 4. The cooled inlet is described in reference 5.

In tests with the adiabatic inlet, the velocity boundary layer developed over the length of 17.0 inches (43.2 cm). Velocity profile measurements in the inlet are presented in references 2 and 3. The thermal boundary layer started to develop at the entrance of the nozzle where a step change in wall temperature occurred.

In the cooled inlet, the velocity boundary layer developed over the length of 37.6 inches (95.5 cm). Cooling was provided for a length of 24.2 inches (61.5 cm) at the downstream end of the inlet. In this case, the thermal boundary layer was well estab-

lished and turbulent at the nozzle entrance. The velocity and thermal boundary layer measurements in the cooled inlet are presented in reference 5.

Nozzle

The 30° half-angle of convergence by 15° half-angle of divergence (30°-15° C-D) water-cooled conical nozzle of reference 2 was used in the investigation. Details of this nozzle are also presented in figure 1. The nozzle had a nominal throat diameter and throat radius of curvature of 1.5 inches (3.8 cm). Velocity and temperature boundary layer surveys were obtained at three stations in the supersonic portion of the nozzle. The free-stream Mach numbers at these stations were 2.1, 3.7, and 4.4.

INSTRUMENTATION

Boundary Layer Probes

Pressure. - A photograph of the boundary layer pressure probe is given in figure 2. The probe tip, shown in the inset, had a nominal tip height of 0.002 inch (0.005 cm) and width of 0.030 inch (0.076 cm). The length from the centerline of the supporting shaft to the tip of the probe was 0.6 inch (1.5 cm). The tip was fabricated from AISI 410 stainless steel.

The pressure probe was driven by a motorized actuator having a span of 0.5 inch (1.3 cm). Contact of the probe with the wall was established by means of an electrical shorting circuit. The wall position provided the reference condition for the displacement measurements. The accuracy of the displacement measurements for the pressure probe is expected to be within 0.001 inch (0.003 cm).

Temperature. - The temperature probe, shown in figure 3, incorporated a Chromel-Alumel thermocouple having an open ball junction (refer to the inset in fig. 3). The ball diameter was nominally 0.003 inch (0.008 cm). The thermocouple sheath, which contacted the wall at the termination of a traverse, had a nominal diameter of 0.008 inch (0.020 cm).

A 0.5-inch (1.3-cm) actuator was used to drive the temperature probe in all tests except for the Mach 3.7 and 4.4 surveys with the cooled inlet. The thermal boundary layer thickness under the latter conditions necessitated the use of an actuator having a greater traversing length. An actuator having a 1.0-inch (2.5-cm) span was used in these tests. The displacement error associated with this actuator was within 0.002 inch (0.005 cm).

Wall Temperature

Wall temperatures used in the analysis of the boundary layer temperature profiles were determined from heat flux meters of the type described in reference 5. Steady-state temperature measurements on the heat meter were incorporated in the Fourier heat conduction equation to determine both the gas-side wall temperature and the local heat transfer rate per unit area.

DATA REDUCTION

Boundary Layer Velocity and Stagnation Temperature

A calibration of the boundary layer pressure probe in subsonic flow indicated a value of recovery ratio $P_r/P_t = 1.0$ over a Mach number range of $0 < M < 1.0$. Subsonic Mach numbers were computed from the measured stagnation pressure P_t and wall static pressure P_w according to the following relation:

$$\frac{P_t}{P_w} = \left(1 + \frac{\gamma - 1}{2} M^2\right)^{\gamma/(\gamma-1)} \tag{1}$$

Equation (1) is valid for isentropic flow of a perfect gas assuming the pressure at the wall P_w is equal to the local static pressure P_s.

In the supersonic portion of the boundary layer, normal shock relations for adiabatic flow of a perfect gas were assumed applicable. Since the normal shock relations imply subsonic Mach numbers at the probe, the probe recovery ratio was assumed equal to 1.0 as represented by the subsonic calibration. The supersonic Mach number was computed from the Rayleigh pitot formula

$$\frac{P_{t-2}}{P_w} = \left(\frac{\gamma + 1}{2} M^2\right)^{\gamma/(\gamma-1)} \left[\frac{\gamma + 1}{2\gamma M^2 - (\gamma - 1)}\right]^{1/(\gamma-1)} \tag{2}$$

Again, the pressure at the wall P_w was assumed equal to the local static pressure in the boundary layer P_s.

The recovery temperature in the boundary layer which was measured with the temperature probe was converted to a local stagnation temperature by accounting for the recovery ratio T_r/T_t as discussed in the appendix. Calibration of the temperature probe

revealed that the recovery ratio is primarily a function of Mach number in subsonic flow. In supersonic flow the local stagnation pressure upstream of the normal shock P_{t-1} as well as the Mach number entered the calculation of recovery ratio. The parametric value of stagnation pressure P_{t-1} was calculated from the following normal shock relation valid for adiabatic flow of a perfect gas:

$$\frac{P_{t-1}}{P_{t-2}} = \left[\frac{(\gamma + 1)M^2}{(\gamma - 1)M^2 + 2}\right]^{-\gamma/(\gamma-1)} \left[\frac{\gamma + 1}{2\gamma M^2 - (\gamma - 1)}\right]^{-1/(\gamma-1)} \tag{3}$$

where P_{t-2} is the pressure sensed by the probe.

A knowledge of the local Mach number and stagnation temperature is sufficient to yield the value of static temperature T_s which can be determined from the adiabatic perfect gas relation

$$\frac{T_t}{T_s} = 1 + \frac{\gamma - 1}{2} M^2 \tag{4}$$

The local velocity in the boundary layer was calculated from the relation

$$u = \sqrt{\gamma R T_s}\, M \tag{5}$$

Method of Determining the Edge of the Boundary Layer

The following method of treating the experimental boundary layer data essentially follows established conventions and is particularly appropriate to the Bartz (ref. 6) theory. The edge conditions used to define the thickness of the layer are based on some nominal fraction (usually 0.99) of the free-stream velocity u_∞ or stagnation temperature T_0. According to this convention, the boundary layer comprises nearly all of the fluid within the region defined by $\partial u/\partial y \neq 0$ or $\partial T_t/\partial_y \neq 0$.

The velocity profiles will be presented in terms of a normalized velocity ratio u/u_e plotted as a function of normalized distance y/δ. The velocity boundary layer thickness δ is hereinafter defined as the distance from the wall y in which the velocity u_e is equal to 99 percent of the free-stream velocity.

The temperature profiles will be presented in terms of the temperature difference ratio $(T_t - T_w)/(T_{t,e} - T_w)$ plotted as a function of normalized distance y/Δ. The thermal boundary layer thickness Δ is defined as the distance from the wall y in which

the stagnation temperature $T_{t,e}$ is equal to 99 percent of the free-stream total temperature. The wall temperature T_w was determined from the heat flux meter as discussed in reference 5.

The momentum and displacement thicknesses, θ and δ^*, respectively, were computed according to the definitions

$$\theta \equiv \int_0^{\zeta} \frac{\rho u}{\rho_e u_e}\left(1 - \frac{u}{u_e}\right)dy \tag{6}$$

and

$$\delta^* \equiv \int_0^{\zeta} \left(1 - \frac{\rho u}{\rho_e u_e}\right) dy \tag{7}$$

The distance ζ was equal to the larger of the values δ and Δ.

The values of θ and δ^* were also computed for an upper limit of $\zeta = y_\infty$ in equations (6) and (7). For these calculations the corresponding values of ρ_e and u_e in equations (6) and (7) were the free-stream values ρ_∞ and u_∞, respectively.

Dimensional Profiles

The distributions of velocity ratio u/u_e and temperature difference ratio $(T_t - T_w)/(T_{t,e} - T_w)$ will also be presented as functions of the distance y which is the dimensional distance from the wall. The purpose of these distributions is to show the experimental profiles in terms of the actual distance rather than the nondimensional variable y/Δ since the boundary layer thickness Δ is often a rather ambiguous quantity. It must be acknowledged that mismatches of power law profiles to the data may be due in part to improper estimates of the thickness Δ. However, as mentioned previously, the conventional flat-plate definition of the edge of the boundary layer is used in this study because of its compatibility with the Bartz (ref. 6) profile assumption.

BOUNDARY LAYER THEORIES

Experimental values of momentum and displacement thickness are compared with predictions based on the integral boundary layer theories of Bartz (ref. 6) and Sasman and Cresci (ref. 7). Only the principal features of these analyses will be presented in this report.

Bartz Method (Ref. 6)

The Bartz integral boundary layer theory of reference 6 essentially involves the simultaneous solution of the integral momentum and energy equation assuming 1/7-power profiles for velocity and temperature difference, Coles friction law, and the von Kármán form of Reynolds analogy. Two basic options, provided in this program, concern the selection of an interaction exponent and method of evaluating the diabatic skin-friction coefficient.

The interaction exponent n relates the Stanton number for unequal momentum and energy thicknesses to that for equal thicknesses by a factor of $(\varphi/\theta)^n$. The normal range of values for n is from 0 to 0.25. In reference 4 it was shown that the values of n greatly influenced the theoretical value of throat heat transfer coefficient. A value of $n = 0$ provided the best predictions of experimental throat heat transfer for a variety of inlet nozzle combinations. In this investigation, the effect of n on the theoretical momentum and displacement thicknesses in the supersonic end of the nozzle was negligible. A value of $n = 0$ was assumed in the Bartz theory except in a few cases which will be used to demonstrate the insensitivity of the boundary layer thicknesses to n.

The diabatic skin-friction coefficient c_f was assumed equal to the adiabatic value $c_{f,ad}$ which is obtained when $T_w = T_{ad}$. The value of $c_{f,ad}$ was obtained from the Coles friction law and is based on free-stream gas properties rather than a film temperature.

Sasman-Cresci Method (Ref. 7)

The Sasman-Cresci boundary layer analysis, presented in reference 7, entails the simultaneous solution of the integral momentum and moment of momentum equations. Additional relations used in solving the equations include the Ludwieg-Tillman skin-friction law and an empirical approximation for the shear stress distribution across the boundary layer.

Theoretical Initialization and Input

Calculations of the boundary layer development in the nozzle will generally be based on initial conditions at the nozzle entrance. Therefore, the theoretical boundary layer in the supersonic flow field will reflect the influence of the highly accelerated subsonic flow. The nozzle entrance boundary layer thicknesses were determined from measurements in the pipe inlet which were extrapolated to the nozzle entrance by means of the Bartz analysis. These initial thicknesses along with the fundamental input quantities are given in table I.

Additional calculations were made with the Sasman-Cresci theory using the Bartz predictions of throat momentum thickness and initializing the calculations at the throat. These calculations were performed when the throat values of momentum and displacement thickness from the two theories differed appreciably.

RESULTS

Velocity Profiles

Velocity profiles obtained in tests with the adiabatic and cooled inlets are presented in figures 4, 5, and 6 for Mach numbers of 2.1, 3.7, and 4.4, respectively. These results are also tabulated in tables II to VII. The 1/7-power profile, assumed in the Bartz theory (ref. 6), is presented in part (a) of these figures to provide a reference for the nondimensional boundary layer velocity distributions. The experimental velocity profiles in tests with the adiabatic inlet are in good agreement with the 1/7-power law at the downstream stations having Mach numbers of 3.7 and 4.4 (figs. 5(a) and 6(a), respectively). However, the profile at Mach 2.1, shown in figure 4(a) was rather unique from the standpoint of a slight depression at $y/\delta = 0.5$. Examination of figure 4(a) also reveals a similar type of depression at $y/\delta = 0.13$ for the profile obtained in tests with a cooled inlet. Figure 4(b) indicates that this irregularity in the profile occurred at $y \approx 0.012$ inch (0.030 cm); that is, the true distance from the wall in which the depression occurred was essentially independent of the degree of inlet cooling.

The distortion of these profiles is probably attributable to flow separation at the tangent point ($x/d^* = 0.268$) which is in close proximity to the measuring station (refer to fig. 1). This tangent point is formed by the intersection of the circular arc throat and the conical effuser. The flow separation phenomenon occurring at the tangent point in conical nozzles as well as the accompanying effect on heat transfer has been discussed in reference 8.

In tests with the cooled inlet, the nondimensional boundary layer velocity profiles at

the three supersonic stations were appreciably different than the 1/7-power profile (refer to figs. 4(a), 5(a), and 6(a)). Examination of the corresponding dimensional profiles (figs. 4(b), 5(b), and 6(b)) indicates that the principal reason for these differences in the profiles concerns the large differences in thickness δ resulting from the different levels of inlet cooling. Much larger values of δ were obtained in the supersonic flow when the inlet was cooled.

The large values of velocity boundary layer thickness δ correspondingly occurred when the thermal boundary layer thickness Δ greatly exceeded the distance δ_M where the Mach number (pressure ratio P_{t-2}/P_s) became a constant. This is illustrated typically in figure 7 which is based on the results at Mach 3.7 for tests with the cooled inlet.

The experimental Mach number and temperature profiles at the Mach 3.7 station are shown in figure 7(a). The local Mach number M reaches the free-stream value M_∞ at a distance $\delta_M = 0.111$ inch (0.282 cm). However, the local stagnation temperature T_t approaches the edge value of temperature $T_{t,e}$ at a distance ($\Delta = 0.408$ in. (1.04 cm)) which is nearly four times greater than δ_M. In the region defined by $\delta_M \leq y \leq \Delta$, the static temperature varies according to equation (4). Since the Mach number is constant over $\Delta_M \leq y \leq \Delta$, the velocity must vary in this region. This variation in velocity, given by equation (5), is shown in figure 7(b). Although the value of velocity boundary layer thickness δ is less than the thermal boundary layer thickness Δ, it is clear that the temperature variation in this outer region influences the velocity profile.

The 1/7-power profile used in the Bartz method (ref. 6) is also shown in figure 7(b). The theoretical thickness δ compares more favorably with δ_M than with the experimental velocity boundary layer thickness δ. The significance of the differences in these profiles is difficult to determine because the integral boundary layer theory of Bartz (ref. 6) assumes a 1/7-power profile for the temperature as well as the velocity profile. It will be shown that the 1/7-power thermal boundary layer profile was not in agreement with the data. However, since the desired thicknesses (momentum and displacement given by eqs. (6) and (7), respectively) require a knowledge of both the velocity and thermal boundary layer, the respective errors in the assumed profiles can have a compensating or possibly negligible effect. Therefore, from a practical standpoint, the 1/7-power profile assumption may be reasonable for computing deficiency thicknesses, at least for the present operating conditions. Further comments on the profile assumptions will be presented upon comparison of the experimental and theoretical momentum and displacement thicknesses.

Temperature Profiles

Temperature profiles obtained at the three supersonic stations are shown in figures 8 to 10. These results are also tabulated in tables II to VII. Examination of figures 8(a) to 10(a) indicates that the nondimensional profiles obtained in tests with both the adiabatic and cooled inlets were not in agreement with the 1/7-power profile. The principal effect of increasing the thickness of the thermal boundary layer at the nozzle entrance was to increase the thermal boundary layer thickness Δ and, consequently, alter the shape of the profile in the supersonic flow field. The dimensional profiles given in figures 8(b) to 10(b) indicate that in progressing downstream the inner portions of the profiles tend to coincide. For example, at the downstream station (fig. 10(b)), the temperature profiles appear to be the same from the wall to $y \approx 0.040$ inch (0.102 cm). However, large differences are apparent in the outer portion of these profiles, particularly from the standpoint of the thickness Δ. These large differences in Δ resulting from the different inlet thermal boundary layer thicknesses, contribute to the pronounced difference in the shape of the nondimensional profile shown in figure 10(a). Similar results were obtained for the other stations (figs. 8 and 9).

The nondimensional temperature profiles obtained in tests with the cooled inlet differed from both the 1/7-power profile and the profiles measured in tests with the adiabatic inlet. The latter profiles were better described by a 1/4-power law as shown in figures 8(a) to 10(a). The profiles obtained in tests with the cooled inlet cannot be adequately described by such a simple power law model. A pronounced change in the curvature of these profiles can be noted at distances of y/Δ ranging from about 0.15 at Mach 2.1 to 0.30 at Mach 4.4 (figs. 8(a) to 10(a), respectively). This change is equally apparent in the dimensional profiles given in figures 8(b) to 10(b). In general the change in curvature takes place at a distance of δ_M which denotes the thickness of the Mach number layer (distance from the wall in which the pitot pressure attains a constant value). By neglecting the temperature variation in the outer part of the boundary layer ($y > \delta_M$) and defining a new value of thermal boundary layer thickness Δ where $\Delta \approx \delta_M$, the two experimental thermal boundary layer profiles at a given station will exhibit a similarity. That is, the inner portions of the profiles defined by $y \leq \delta_M$ have about the same power-law variation which in the case of the temperature profiles is given approximately by

$$\frac{T_t - T_w}{T_{t,e} - T_w} \propto y^{1/4} \tag{8}$$

The corresponding power law variation for the velocity profiles obtained by neglecting the outerpart of the temperature profile is

$$\frac{u}{u_e} \propto y^{1/7}$$

Incorporation of a 1/4-power law rather than the 1/7-power law for the temperature profile in the Bartz analysis (ref. 6) resulted in negligible differences in the predicted deficiency thicknesses. This will be illustrated in a subsequent section of the report.

Comparison of Experimental and Theoretical Deficiency Thicknesses

In this portion of the report, the experimental momentum and displacement thicknesses will be compared to predictions based on the Bartz (ref. 6) and Sasman-Cresci (ref. 7) theories. The experimental results at each station are denoted by a shaded and open symbol. These symbols differentiate between the limits of integration used to establish the deficiency thicknesses. The open symbols indicate that the integration was performed over a distance ζ which was equal to the larger of the values δ and Δ (refer to eqs. (6) and (7)). The shaded symbols correspond to integrations over the range of $0 \leq y \leq y_\infty$ where y_∞ is any point in the free stream. In the boundary layer of zero-pressure-gradient flows the difference in the results evolving from the different upper limits of integration is usually negligible. However, in the accelerated flow of a nozzle, the edge conditions of the turbulent boundary layer are often rather ambiguous quantities (ref. 5). In this report the difference in the results for the two upper limits of integration will be treated as an experimental uncertainty. The theoretical results will be compared to deficiency thicknesses within an uncertainty band formed by the line joining the two data points at each station.

The theoretical distributions of deficiency thickness were obtained by initializing the calculations at the nozzle entrance in accordance with the values given in table I(b). The local values of wall temperature and static pressure, which are also required in the boundary layer calculations, are given in table I(a).

Momentum thickness distributions. - Experimental and theoretical distributions of momentum thickness are presented in figures 11 and 12 for tests with an adiabatic and cooled inlet, respectively. The results obtained in tests with an adiabatic inlet (fig. 11) indicate that both theories were in good agreement in the subsonic and throat portions of the nozzle; however, a modest divergence in the results occurs in the supersonic portion of the nozzle ($x/d^* > 0$). The results of figure 12, corresponding to tests with a cooled inlet, reveal a greater difference in the theoretical thicknesses throughout the nozzle. At the downstream survey station ($x/d^* = 6.381$), the difference in predicted values of θ was about 14 and 6 percent of the mean levels for tests with the adiabatic and cooled inlets, respectively. In the supersonic flow, the Sasman-Cresci method (ref. 7) pre-

dicted higher values of θ than the Bartz theory (ref. 6) in tests with the adiabatic inlet, whereas the converse of these results applies in the case of tests with a cooled inlet.

The theoretical distributions of momentum thickness are within or slightly below the values within the uncertainty band. The Sasman-Cresci theory (ref. 7) provided better agreement with the experimental values of θ obtained in tests with an adiabatic inlet (fig. 11), but the Bartz method (ref. 6) yielded a better prediction of θ in tests with the cooled inlet (fig. 12). The Bartz theory was not more than 18 percent below the experimental values of θ with the worst agreement occurring at the downstream station (fig. 11). The Sasman-Cresci theory also yielded predictions within about 18 percent of the experimental values as shown in figure 12.

Based on the relative agreement between the theories and experiments it is difficult to preclude one method in favor of the other analysis. Perhaps, however, the greatest significance of the aforementioned results evolves from the abilities of the two theories to account for the experimentally observed change in θ which accompanied the change in inlet cooling. This change in the experimental values of θ can be observed by comparing figures 11 and 12. At a given station larger values of θ were observed when the inlet was cooled. Comparison of figures 11 and 12 also indicates that the Sasman-Cresci theory (ref. 7) did not account for the effects of different inlet thermal boundary layers on the θ-distribution in supersonic flow. The Bartz theory (ref. 6) revealed a small difference the θ-distribution which was consistent with the experimental results. The ability of the Bartz method (ref. 6) to comprehend the effects of different thermal boundary layers on the values of θ lends credence in application of the theory for calculations of θ in supersonic flows, particularly when a significant thermal history is associated with the boundary layer.

Displacement thickness distributions. - The theoretical distributions of displacement thickness δ^*, presented in figures 13 and 14, exhibit a greater divergence in the supersonic portion of the nozzle than the previously discussed momentum thickness distributions. For instance, at the downstream survey station, corresponding to a nominal Mach number of 4.4, theoretical values of δ^* differ by about 20 percent of the mean value for both the adiabatic and cooled inlet tests.

The Bartz theory (ref. 6) equaled or slightly underpredicted the experimental values of δ^* and the Sasman-Cresci theory (ref. 7) overpredicted the experimental results as shown in figures 13 and 14. It is interesting to note the relative change in the theoretical and experimental values of δ^* corresponding to the change in inlet configuration. With the exception of experimental values of δ^* at the downstream station, a slight reduction in thickness was apparent upon replacing the adiabatic inlet with a cooled configuration. The Bartz theory (ref. 6) predicted this observed trend which is most apparent at the upstream stations; however, the Sasman-Cresci theory (ref. 7) indicated no change in δ^* with a change in the thermal boundary layer. At the downstream sur-

vey station the Sasman-Cresci theory (ref. 7) yielded values of δ^* which were about 25 percent higher than the upper limit of values within the experimental uncertainty band (fig. 14). Predictions based on the Bartz theory were about 16 percent lower than the lower limit of values within the uncertainty band (fig. 14).

Effect of Varying the Interaction Exponent in the Bartz Theory (Ref. 6)

The distributions of θ (fig. 11) and δ^* (fig. 13) obtained from the Bartz method of reference 6 are representative of two values of interaction exponents n, namely, $n = 0$ and $n = 0.25$. As noted in the aforementioned figures, the variation in this exponent had no effect on the predicted distributions of θ and a negligible effect on the theoretical distributions of δ^*. Therefore, in calculations of δ^* and θ the value of n used in the theory is of little consequence; however, in calculations of heat transfer rates the value of n becomes very important as was shown in references 4 and 6. Reference 6 should be consulted for further details concerning the interaction exponent.

Predictions Based on Initial Values of Deficiency Thicknesses at Throat

In many applications of boundary layer analyses it is desirable to initiate the calculations at the throat of the nozzle where the boundary layer is very thin. It is important, therefore, to determine the sensitivity of the calculation to the initial values of boundary layer thickness. A demonstration of this sensitivity is presented in figures 12 and 14 where the upstream, and, consequently, the throat values of θ and δ^* differed appreciably. The Sasman-Cresci theory (ref. 7) was initiated at the throat ($x/d^* = 0$) with the value of θ determined from the Bartz method (ref. 6). As shown in figure 12, the theoretical values of θ determined from the Sasman-Cresci theory (ref. 7) rapidly converged to approximately the values obtained from the full nozzle calculation thus indicating an insensitivity to the initial value of θ. A rapid convergence in the corresponding distributions of δ^* can be noted in figure 14.

The Bartz method (ref. 6) initiated on the basis of the Sasman-Cresci throat value of θ also produced a rapid convergence to the originally calculated distribution. This latter result is not shown in order to preserve clarity in figures 12 and 14.

Effect of Varying the Power Law on the Temperature Profile in the Bartz Theory (Ref. 6)

In the previous discussion of the velocity and temperature profiles it was concluded that, upon neglecting the region of the boundary layer corresponding to $y > \delta_M$, the temperature and velocity profiles could be described by 1/4- and 1/7-power laws, respectively. These profiles appeared to be independent of the amount of inlet cooling. In reference 4, both the temperature and velocity profiles in the subsonic portion of the present nozzle were described by a 1/7-power law. These results for subsonic and supersonic flow suggest a new boundary layer model leading to a two-part calculation in the nozzle. The first part of the calculation consists of applying the Bartz theory (ref. 6) to the subsonic portion of the nozzle. The second part of the calculation requires re-initialization of the theory at the nozzle throat; however the power associated with the temperature profile is altered from 1/7 to 1/4 to be more consistent with the observed profiles of this investigation.

In performing the previous calculation it was necessary to establish a compatibility of initial values of δ^* and θ with the calculated values at the throat. Obviously, not all conditions at the throat can be matched since the change in temperature profile necessarily changes the various thicknesses. In the Bartz theory (ref. 6) the boundary layer input consists of the values of θ and Δ/δ. Therefore, in order to match the throat values of θ and δ^* resulting from the upstream calculation, it was necessary to iterate in the second part of the analysis on the basis of Δ/δ until matching of θ and δ^* was achieved.

The results of the two-part calculation are shown in figures 12 and 14. In figure 12 it can be observed that no change occurred in the distribution of θ when the temperature power law was altered. A very slight change in the δ^* distribution accompanied this change in the power law as shown in figure 14. The change, however, was in the direction of reduced levels of δ^* which produces a greater deviation from the experimental results.

SUMMARY OF RESULTS

Time-mean velocity and temperature profiles in a turbulent boundary layer were measured at three stations in the supersonic portion of a 30° - 15° C-D nozzle. The nominal Mach number range for the boundary layer surveys was from 2.1 to 4.4. The Reynolds number based on diameter was about 5.5×10^6 and 3.5×10^6 at the upstream and downstream stations, respectively. Tests were performed with an adiabatic and a

cooled inlet in order to change the thermal boundary layer thickness at the nozzle entrance. The ratio of wall-to-stagnation temperature, which was nearly independent of the inlet configuration, was about 0.8 at Mach 2.1 and about 0.6 Mach 4.4. The experimental results were compared to theoretical predictions based on the methods of Bartz and Sasman-Cresci. The most significant results of this investigation can be summarized in order of prominence as follows:

1. The thermal boundary layer profiles in the supersonic portion of the nozzle were not described by a 1/7-power profile which is often associated with the turbulent boundary layer in a pipe. The velocity profiles were described by the 1/7-power law when the thermal and Mach number layers were of comparable thickness. However, when the thermal boundary layer thickness greatly exceeded the thickness of the Mach number layer, the velocity profile deviated from the conventional power profile. These latter results were observed in tests with a cooled inlet which produced a thick thermal boundary layer at the nozzle entrance.

2. Predictions of momentum and displacement thickness based on the Bartz and Sasman-Cresci methods revealed modest differences in momentum thickness and pronounced differences in displacement thickness with increasing supersonic Mach number.

3. The agreement between experimental and theoretical values of momentum thickness was generally within ±18 percent of the experimental uncertainty band. The Sasman-Cresci method tended to overpredict the experimental values of displacement thickness whereas the Bartz theory underpredicted the observed results. At the downstream station, the predictions were within plus 25 percent and minus 16 percent of the experimental uncertainty band.

4. The Sasman-Cresci theory did not account for changes in the thermal boundary layer history imposed by the use of an adiabatic and a cooled inlet. This was noted as a result of comparing the predictions of momentum and displacement thickness for tests having an adiabatic inlet with the distributions corresponding to tests having a cooled inlet. The Sasman-Cresci predictions of the deficiency thicknesses were identical for the two tests. The Bartz method qualitatively predicted the experimental changes in deficiency thickness resulting from different inlet thermal boundary layers.

CONCLUDING REMARKS

The results of this investigation tend to emphasize the importance of the inlet thermal boundary layer relative to the displacement and momentum thickness distributions in the supersonic part of the nozzle. It has been known that differences in the thickness of the inlet momentum boundary layer are essentially eradicated by the strong accelerating forces in the subsonic and throat portions of the nozzle. Differences in

inlet thermal boundary layer thickness are not erased by this acceleration. These initial differences are reflected in the profiles and deficiency thicknesses in the supersonic flow.

The ability of a theory to account for the complex development of the momentum and thermal boundary layers is important, particularly in thrustor nozzles. With this consideration in mind, it may be more desirable to use an analysis of the Bartz type in predictions of the momentum and displacement thicknesses since it appeared to account for the effects of different thermal histories, at least for the conditions of the present investigation. For applications such as the design of adiabatic wall nozzles of the type used in certain wind tunnels, the Sasman-Cresci type analysis may provide equally good or better predictions of the deficiency thicknesses. An illustration of the high degree of accuracy of the latter theory in the case of an adiabatic wall nozzle is presented in reference 7.

Lewis Research Center,
National Aeronautics and Space Administration,
Cleveland, Ohio, April 16, 1969,
129-01-05-19-22.

APPENDIX - RECOVERY CHARACTERISTICS OF TEMPERATURE PROBE

The recovery characteristics of the temperature probe, shown in figure 3, will be presented in terms of the temperature recovery ratio T_r/T_t which, to a first order, varies with the Mach number M. The calibration of the probe was performed in a free jet operating at ambient temperature over a range of subsonic Mach numbers and at Mach 1.4. The results of the subsonic and Mach 1.4 calibrations are shown in figure 15 as regions I and II, respectively. The ±1/2 percent band attached to the temperature recovery ratio at Mach 1.4 indicates the sensitivity to the stagnation pressure level.

The data points in region III of figure 15 were obtained in the test nozzle. The shaded symbols represent temperature recovery ratios measured with the probe in the free stream. These data correspond to operation at the design stagnation pressure and temperature, 300 pounds per square inch (207 N/cm^2) absolute and 970° R (539 K), respectively. The upper line in figure 15 has been faired through these data and represents a reference level for subsequent calculations of temperature recovery ratio at off-design pressures.

The calculated curves of region III, figure 15, were based on the experimental variation of temperature recovery ratio with stagnation pressure P_{t-1} at Mach 3.7. If a functional relation of the type used in reference 9 was assumed, a curve fit of the data yielded the following expression for the temperature recovery ratio:

$$\frac{T_r}{T_t} = \left(\frac{T_r}{T_t}\right)_{ref} - \left[1 - \left(\frac{T_r}{T_t}\right)_{ref}\right]\left[\left(\frac{P_{t-1}}{P_{t-1,ref}}\right)^{-0.16} - 1\right] \tag{A1}$$

The reference quantities in equation (A1) were obtained from the reference curve in figure 15. As noted in equation (A1), the recovery temperature ratio is a function of pressure ratio raised to a power of -0.16. This is approximately the same function that was obtained in reference 9 for unshielded spike probes.

The variation of T_r/T_t with P_{t-1} in region II of figure 15 was obtained by linear extrapolation between Mach numbers of 1.0 and 2.0. The resulting variation of T_r/T_t with M and P_{t-1} in region II is given approximately by

$$\frac{T_r}{T_t} = -0.065\, P_{t-1}^{-0.316}\,(M - 1.0) + 0.9805 \tag{A2}$$

The variation of temperature recovery ratio in region I of figure 15 was obtained from the curve faired through the free-jet calibration data. The effect of stagnation

pressure level on recovery ratio was neglected in this region.

The effect of temperature level on the temperature recovery ratio was assumed negligible. The change in temperature recovery ratio with temperature level at Mach 2.1 and 3.7 was less than 1 percent for free-stream stagnation temperatures between 550° and 970° R (308 and 539 K).

REFERENCES

1. Rotta, J. C.: Critical Review of Experimental Heat Transfer Coefficients and Temperature Distributions in Turbulent Boundary Layers at Supersonic and Hypersonic Flow. NASA TT F-10,905, 1967.

2. Boldman, Donald R.; and Schmidt, James F.; and Fortini, Anthony: Turbulence, Heat-Transfer, and Boundary Layer Measurements in a Conical Nozzle with a Controlled Inlet Velocity Profile. NASA TN D-3221, 1966.

3. Boldman, D. R.; Schmidt, J. F.; and Ehlers, R. C.: Effect of Uncooled Inlet Length and Nozzle Convergence Angle on the Turbulent Boundary Layer and Heat Transfer in Conical Nozzles Operating With Air. J. Heat Transfer, vol. 89, no. 4, Nov. 1967, pp. 341-350.

4. Boldman, Donald R.; Neumann, Harvey E.; and Schmidt, James F.: Heat Transfer in 30° and 60° Half-Angle of Convergence Nozzles With Various Diameter Uncooled Pipe Inlets. NASA TN D-4177, 1967.

5. Boldman, Donald R.; Schmidt, James F.; and Gallagher, Anne K.: Laminarization of a Turbulent Boundary Layer as Observed from Heat-Transfer and Boundary Layer Measurements in Conical Nozzles. NASA TN D-4788, 1968.

6. Bartz, D. R.: Turbulent Boundary-Layer Heat Transfer from Rapidly Accelerating Flow of Rocket Combustion Gases and of Heated Air. Advances in Heat Transfer. Vol. 2. James P. Hartnett and Thomas F. Irvine, Jr., eds., Academic Press, 1965, pp. 1-108.

7. Sasman, Philip K.; and Cresci, Robert J.: Compressible Turbulent Boundary Layer With Pressure Gradient and Heat Transfer. AIAA J., vol. 4, no. 1, Jan. 1966, pp. 19-25.

8. Back, L. H.; Massier, P. F.; and Cuffel, R. F.: Flow Phenomena and Convective Heat Transfer in a Conical Supersonic Nozzle. J. Spacecraft Rockets, vol. 4, no. 8, Aug. 1967, pp. 1040-1047.

9. Stickney, Truman M.: Recovery and Time-Response Characteristics of Six Thermocouple Probes in Subsonic and Supersonic Flow. NACA TN 3455, 1955.

TABLE I. - INPUT AND INITIAL BOUNDARY LAYER THICKNESSES

USED IN THEORETICAL CALCULATIONS

[Stagnation temperature $T_0 \approx 970^{\circ}$ R (539 K); stagnation pressure $P_0 \approx 300$ psia (207 N/cm^2); throat diameter d* = 1.492 in. (3.790 cm).]

(a) Experimental input

Station	Axial distance, z		Diameter, d		Nondimensional distance, x/d*	Pressure ratio, P_w/P_0	Wall temperature, T_w			
							Adiabatic inlet		Cooled inlet	
	in.	cm	in.	cm			$^{\circ}$R	K	$^{\circ}$R	K
1	0.000	0.000	6.500	16.510	-3.175	0.99932	700	389	674	374
2	.222	.564	6.250	15.875	-3.026	.99946	702	390	677	376
3	1.222	3.104	5.092	12.934	-2.356	.99847	712	396	701	389
4	2.225	5.652	3.934	9.992	-1.684	.99565	763	424	755	420
5	2.579	6.551	3.528	8.961	-1.446	.99325	780	433	763	424
6	2.925	7.430	3.128	7.945	-1.214	.98887	793	441	770	428
7	3.277	8.324	2.722	6.914	-.979	.9804	806	448	782	435
8	3.627	9.213	2.316	5.883	-.744	.9624	824	458	800	444
9	4.124	10.475	1.760	4.470	-.411	.8399	847	471	823	457
10	4.562	11.587	1.510	3.835	-.117	.5733	838	466	823	457
11	4.737	12.032	1.492	3.790	0	.4600	831	462	824	458
12	4.867	12.362	1.502	3.815	.087	.3733	824	458	803	446
13	4.992	12.680	1.540	3.912	.171	.2785	819	455	794	441
14	5.129	13.028	1.604	4.074	.263	.2084	809	449	786	437
15	5.371	13.642	1.732	4.399	.425	.1820	799	444	782	435
[a]16	5.958	15.133	2.042	5.187	.818	.1125	776	431	765	425
17	7.473	18.981	2.858	7.259	1.834	.0375	726	403	716	398
[a]18	10.205	25.921	4.322	10.978	3.665	.0094	621	345	631	351
19	12.938	32.863	5.792	14.712	5.497	.0038	578	321	579	322
[a]20	14.257	36.213	6.504	16.520	6.381	------	---	---	---	---
21	15.769	40.053	7.320	18.593	7.394	.0024	569	316	570	317

(b) Boundary layer thickness at nozzle entrance

Station	Boundary layer thickness											
	Adiabatic inlet						Cooled inlet					
	Momentum, θ		Velocity, δ		Temperature, Δ		Momentum, θ		Velocity, δ		Temperature, Δ	
	in.	cm	in.	cm	in.	cm	in.	cm	in.	cm	in.	cm
1	0.0343	0.0871	0.334	0.848	0.00334	0.00848	0.063	0.160	0.610	1.549	0.552	1.402

[a]Denotes stations where boundary layer surveys were obtained.

TABLE II. - BOUNDARY LAYER SURVEY AT A NOMINAL MACH NUMBER OF 2.1 FOR ADIABATIC INLET

[Free-stream velocity u_∞ = 2319 ft/sec (706 m/sec); wall temperature T_w = 788° R (438 K); free-stream stagnation temperature T_0 = 973° R (541 K); edge stagnation temperature $T_{t,e}$ = 964° R (535 K); velocity boundary layer thickness δ = 0.021 in. (0.053 cm); temperature boundary layer thickness Δ = 0.039 in. (0.099 cm).]

Integration to edge condition				Integration to free-stream condition			
Momentum, θ		Displacement, δ^*		Momentum, θ		Displacement, δ^*	
in.	cm	in.	cm	in.	cm	in.	cm
0.0014	0.0036	0.0034	0.0086	0.0030	0.0076	0.0040	0.0102

Distance from nozzle wall, y		Local static temperature, T		Local stagnation temperature, T_t		Local velocity, u		Local Mach number, M	Velocity ratio, u/u_∞	Temperature difference ratio, $\frac{T_t - T_w}{T_0 - T_w}$	Distance ratio, y/δ	Velocity ratio, u/u_e	Distance ratio, y/Δ	Temperature difference ratio, $\frac{T_t - T_w}{T_{t,e} - T_w}$
in.	cm	°R	K	°R	K	ft/sec	m/sec							
0.0012	0.0032	694	386	851	473	1374	418	1.1	0.592	0.342	0.059	0.598	0.032	0.361
0.0024	0.0062	659	366	860	478	1554	473	1.2	0.670	0.388	0.115	0.677	0.063	0.409
0.0034	0.0088	634	352	867	482	1675	510	1.4	0.722	0.426	0.162	0.730	0.089	0.450
0.0044	0.0113	609	338	874	486	1786	544	1.5	0.770	0.464	0.209	0.778	0.115	0.490
0.0064	0.0164	566	315	888	494	1967	599	1.7	0.848	0.541	0.302	0.857	0.167	0.571
0.0084	0.0215	532	295	902	501	2110	643	1.9	0.910	0.617	0.396	0.919	0.219	0.651
0.0089	0.0227	525	292	906	503	2139	651	1.9	0.923	0.636	0.420	0.932	0.232	0.672
0.0094	0.0240	519	289	910	505	2165	659	1.9	0.934	0.655	0.443	0.943	0.245	0.692
0.0099	0.0253	518	288	913	507	2178	663	2.0	0.940	0.674	0.467	0.945	0.257	0.712
0.0104	0.0265	521	290	917	509	2179	664	1.9	0.940	0.694	0.490	0.949	0.270	0.732
0.0109	0.0278	526	292	920	511	2176	663	1.9	0.938	0.713	0.514	0.948	0.283	0.752
0.0114	0.0291	528	294	924	513	2179	664	1.9	0.940	0.732	0.537	0.949	0.296	0.772
0.0119	0.0304	529	294	926	514	2184	665	1.9	0.942	0.741	0.560	0.951	0.309	0.782
0.0124	0.0316	527	293	927	515	2192	668	1.9	0.946	0.750	0.584	0.955	0.322	0.791
0.0134	0.0342	523	290	930	517	2213	674	2.0	0.954	0.767	0.631	0.964	0.348	0.809
0.0144	0.0367	520	289	933	519	2229	679	2.0	0.961	0.784	0.678	0.971	0.374	0.827
0.0154	0.0392	517	287	937	520	2246	684	2.0	0.969	0.801	0.725	0.978	0.400	0.845
0.0164	0.0418	515	286	940	522	2258	688	2.0	0.974	0.818	0.771	0.984	0.426	0.863
0.0184	0.0469	514	285	946	526	2279	694	2.1	0.983	0.852	0.865	0.992	0.477	0.899
0.0204	0.0519	515	286	952	529	2292	698	2.1	0.989	0.886	0.959	0.999	0.529	0.935
0.0209	0.0532	515	286	954	530	2295	699	2.1	0.990	0.894	0.982	1.000	0.542	0.944
0.0404	0.1027	521	290	965	536	2308	703	2.1	0.996	0.953	1.897	1.000	1.047	1.000
0.1897	0.4820	526	292	973	540	2318	706	2.1	1.000	0.996	8.899	1.000	4.910	1.000
0.3397	0.8630	526	292	973	541	2319	706	2.1	1.000	1.000	15.933	1.000	8.792	1.000

TABLE III. - BOUNDARY LAYER SURVEY AT A NOMINAL MACH NUMBER OF 3.7 FOR ADIABATIC INLET

[Free-stream velocity u_∞ = 2925 ft/sec (891 m/sec); wall temperature T_w = 637° R (354 K); free-stream stagnation temperature T_0 = 970° R (539 K); edge stagnation temperature $T_{t,e}$ = 960° R (533 K); velocity boundary layer thickness δ = 0.087 in. (0.221 cm); temperature boundary layer thickness Δ = 0.083 in. (0.211 cm).]

Integration to edge condition				Integration to free-stream condition			
Momentum, θ		Displacement, δ^*		Momentum, θ		Displacement, δ^*	
in.	cm	in.	cm	in.	cm	in.	cm
0.0050	0.013	0.024	0.061	0.0055	0.014	0.026	0.066

Distance from nozzle wall, y		Local static temperature, T		Local stagnation temperature, T_t		Local velocity, u		Local Mach number, M	Velocity ratio, u/u_∞	Temperature difference ratio, $\frac{T_t - T_w}{T_0 - T_w}$	Distance ratio, y/δ	Velocity ratio, u/u_e	Distance ratio, y/Δ	Temperature difference ratio, $\frac{T_t - T_w}{T_{t,e} - T_w}$
in.	cm	°R	K	°R	K	ft/sec	m/sec							
0.0012	0.0032	566	315	740	411	1444	440	1.2	0.494	0.309	0.014	0.499	0.015	0.318
0.0017	0.0044	553	307	750	417	1538	468	1.3	0.526	0.340	0.020	0.531	0.021	0.350
0.0022	0.0057	539	299	761	423	1632	497	1.4	0.558	0.371	0.026	0.564	0.027	0.383
0.0027	0.0070	527	293	771	428	1713	522	1.5	0.586	0.403	0.031	0.592	0.033	0.415
0.0032	0.0083	516	287	781	434	1786	544	1.6	0.611	0.434	0.037	0.617	0.039	0.447
0.0037	0.0095	505	281	792	440	1854	565	1.7	0.634	0.465	0.043	0.641	0.045	0.479
0.0042	0.0108	501	278	802	446	1901	579	1.7	0.650	0.497	0.049	0.657	0.051	0.511
0.0047	0.0121	491	273	811	450	1960	597	1.8	0.670	0.522	0.054	0.677	0.057	0.538
0.0052	0.0133	485	270	817	454	1995	607	1.8	0.682	0.540	0.060	0.689	0.063	0.556
0.0062	0.0159	467	259	826	459	2078	633	2.0	0.711	0.569	0.072	0.718	0.075	0.586
0.0072	0.0184	452	251	832	462	2135	650	2.0	0.730	0.586	0.083	0.737	0.087	0.603
0.0077	0.0197	445	247	834	463	2161	658	2.1	0.739	0.592	0.089	0.746	0.093	0.610
0.0082	0.0210	441	245	836	464	2179	664	2.1	0.745	0.599	0.094	0.753	0.099	0.617
0.0112	0.0286	422	234	849	472	2264	690	2.2	0.774	0.637	0.129	0.782	0.135	0.656
0.0132	0.0337	413	229	856	476	2307	703	2.3	0.789	0.659	0.152	0.797	0.159	0.679
0.0172	0.0438	397	221	870	483	2382	726	2.4	0.815	0.700	0.198	0.823	0.207	0.721
0.0297	0.0756	359	199	897	498	2542	774	2.7	0.869	0.782	0.341	0.878	0.357	0.806
0.0422	0.1073	327	182	919	510	2667	812	3.0	0.912	0.848	0.484	0.921	0.507	0.873
0.0552	0.1403	301	167	937	520	2762	841	3.2	0.945	0.901	0.633	0.954	0.662	0.928
0.0672	0.1708	283	157	949	527	2829	862	3.4	0.967	0.938	0.770	0.977	0.806	0.967
0.0802	0.2038	268	149	959	533	2880	877	3.6	0.985	0.967	0.919	0.995	0.962	0.996
0.0927	0.2356	260	144	963	535	2907	886	3.7	0.994	0.982	1.062	1.000	1.112	1.000
0.1052	0.2673	258	143	966	537	2917	889	3.7	0.997	0.990	1.205	1.000	1.262	1.000
0.1182	0.3004	257	143	967	537	2920	890	3.7	0.998	0.993	1.354	1.000	1.418	1.000
0.1302	0.3308	257	143	968	538	2922	890	3.7	0.999	0.996	1.492	1.000	1.562	1.000
0.1432	0.3639	257	143	969	538	2923	890	3.7	0.999	0.997	1.641	1.000	1.717	1.000
0.1557	0.3956	257	143	969	538	2924	891	3.7	1.000	0.999	1.784	1.000	1.867	1.000
0.1682	0.4274	257	143	969	538	2924	891	3.7	1.000	0.999	1.927	1.000	2.017	1.000
0.1932	0.4909	257	143	969	539	2925	891	3.7	1.000	1.000	2.213	1.000	2.317	1.000
0.2482	0.6306	257	143	969	539	2925	891	3.7	1.000	1.000	2.843	1.000	2.976	1.000

TABLE IV. - BOUNDARY LAYER SURVEY AT A NOMINAL MACH NUMBER OF 4.4 FOR ADIABATIC INLET

[Free-stream velocity u_∞ = 3043 ft/sec (927 m/sec); wall temperature T_w = 570° R (317 K); free-stream stagnation temperature T_0 = 970° R (539 K); edge stagnation temperature $T_{t,e}$ = 960° R (533 K); velocity boundary layer thickness δ = 0.161 in. (0.409 cm); temperature boundary layer thickness Δ = 0.161 in. (0.409 cm).]

Integration to edge condition				Integration to free-stream condition			
Momentum, θ		Displacement, δ^*		Momentum, θ		Displacement, δ^*	
in.	cm	in.	cm	in.	cm	in.	cm
0.0090	0.0229	0.056	0.142	0.010	0.025	0.061	0.155

Distance from nozzle wall, y		Local static temperature, T		Local stagnation temperature, T_t		Local velocity, u		Local Mach number, M	Velocity ratio, u/u_∞	Temperature difference ratio, $\frac{T_t - T_w}{T_0 - T_w}$	Distance ratio, y/δ	Velocity ratio, u/u_e	Distance ratio, y/Δ	Temperature difference ratio, $\frac{T_t - T_w}{T_{t,e} - T_w}$
in.	cm	°R	K	°R	K	ft/sec	m/sec							
0.0012	0.0032	654	363	694	385	691	210	0.6	0.227	0.309	0.008	0.229	0.008	0.317
0.0030	0.0076	591	328	719	400	1244	379	1.0	0.409	0.374	0.019	0.412	0.019	0.383
0.0032	0.0083	537	299	723	402	1494	455	1.3	0.491	0.383	0.020	0.496	0.020	0.393
0.0052	0.0133	513	285	752	418	1697	517	1.5	0.558	0.457	0.033	0.562	0.033	0.468
0.0072	0.0184	487	270	773	430	1855	565	1.7	0.610	0.508	0.045	0.616	0.045	0.521
0.0092	0.0235	459	255	784	436	1976	602	1.9	0.650	0.536	0.058	0.656	0.057	0.549
0.0132	0.0337	436	242	798	443	2084	635	2.0	0.685	0.570	0.083	0.692	0.082	0.584
0.0172	0.0438	415	230	808	449	2173	662	2.2	0.714	0.595	0.107	0.721	0.107	0.610
0.0232	0.0591	398	221	823	457	2259	688	2.3	0.742	0.632	0.145	0.750	0.144	0.648
0.0282	0.0718	384	214	832	462	2318	706	2.4	0.762	0.655	0.176	0.769	0.175	0.671
0.0412	0.1048	352	196	854	474	2454	748	2.7	0.807	0.710	0.257	0.815	0.256	0.727
0.0652	0.1657	303	168	886	492	2647	806	3.1	0.870	0.791	0.406	0.879	0.405	0.810
0.0862	0.2191	269	150	910	506	2774	845	3.4	0.912	0.851	0.537	0.921	0.535	0.872
0.1032	0.2623	248	138	927	515	2856	870	3.7	0.939	0.894	0.643	0.948	0.640	0.916
0.1212	0.3080	230	128	940	522	2921	890	3.9	0.960	0.927	0.755	0.970	0.752	0.950
0.1417	0.3600	214	119	952	529	2978	907	4.2	0.979	0.957	0.883	0.988	0.879	0.980
0.1497	0.3804	209	116	956	531	2995	912	4.2	0.984	0.966	0.932	0.994	0.928	0.990
0.1592	0.4045	205	114	959	533	3011	917	4.3	0.989	0.974	0.992	0.999	0.987	0.999
0.1672	0.4248	202	112	962	534	3020	920	4.3	0.993	0.980	1.041	1.000	1.037	1.000
0.1732	0.4401	200	111	963	535	3026	922	4.4	0.994	0.982	1.079	1.000	1.074	1.000
0.1782	0.4528	199	111	963	535	3029	923	4.4	0.995	0.984	1.110	1.000	1.105	1.000
0.1832	0.4655	199	110	964	535	3031	923	4.4	0.996	0.985	1.141	1.000	1.136	1.000
0.1972	0.5010	198	110	965	536	3033	924	4.4	0.997	0.987	1.228	1.000	1.223	1.000
0.4832	1.2275	199	110	970	539	3043	927	4.4	1.000	1.000	3.009	1.000	2.996	1.000

TABLE V. - BOUNDARY LAYER SURVEY AT A NOMINAL MACH NUMBER OF 2.1 FOR COOLED INLET

[Free-stream velocity u_∞ = 2324 ft/sec (708 m/sec); wall temperature T_w = 771° R (438 K); free-stream stagnation temperature T_0 = 971° R (541 K); edge stagnation temperature $T_{t,e}$ = 961° R (534 K); velocity boundary layer thickness δ = 0.108 in. (0.274 cm); temperature boundary layer thickness Δ = 0.155 in. (0.394 cm).]

Integration to edge condition				Integration to free-stream condition			
Momentum, θ		Displacement, δ^*		Momentum, θ		Displacement, δ^*	
in.	cm	in.	cm	in.	cm	in.	cm
0.0024	0.0061	0.0019	0.0048	0.0039	0.0099	0.0016	0.0041

Distance from nozzle wall, y		Local static temperature, T		Local stagnation temperature, T_t		Local velocity, u		Local Mach number, M	Velocity ratio, u/u_∞	Temperature difference ratio, $\frac{T_t - T_w}{T_0 - T_w}$	Distance ratio, y/δ	Velocity, ratio, u/u_e	Distance ratio, y/Δ	Temperature difference ratio, $\frac{T_t - T_w}{T_{t,e} - T_w}$
in.	cm	°R	K	°R	K	ft/sec	m/sec							
0.0012	0.0032	695	386	845	470	1344	409	1.0	0.579	0.371	0.012	0.584	0.008	0.390
0.0040	0.0103	619	344	852	473	1673	509	1.4	0.720	0.405	0.038	0.727	0.026	0.425
0.0045	0.0116	606	337	853	474	1722	524	1.4	0.741	0.411	0.042	0.749	0.029	0.432
0.0055	0.0141	585	325	856	476	1805	550	1.5	0.777	0.426	0.051	0.784	0.036	0.447
0.0060	0.0154	574	319	858	477	1845	562	1.6	0.794	0.434	0.056	0.802	0.039	0.456
0.0080	0.0204	544	302	866	481	1968	599	1.7	0.847	0.476	0.075	0.855	0.052	0.500
0.0089	0.0227	528	293	871	484	2028	618	1.8	0.873	0.497	0.083	0.882	0.058	0.523
0.0100	0.0255	507	282	878	488	2110	642	1.9	0.908	0.532	0.093	0.917	0.065	0.560
0.0104	0.0265	502	279	880	489	2133	650	1.9	0.918	0.547	0.097	0.927	0.068	0.575
0.0110	0.0281	496	275	885	492	2161	658	2.0	0.930	0.568	0.102	0.939	0.071	0.597
0.0122	0.0311	487	270	893	496	2209	673	2.0	0.951	0.610	0.114	0.960	0.079	0.642
0.0124	0.0316	487	271	895	497	2213	674	2.0	0.952	0.617	0.115	0.962	0.081	0.649
0.0126	0.0321	488	271	896	498	2215	675	2.0	0.953	0.624	0.117	0.963	0.082	0.656
0.0128	0.0326	489	272	897	499	2215	675	2.0	0.953	0.631	0.119	0.963	0.083	0.663
0.0132	0.0337	494	274	900	500	2208	673	2.0	0.950	0.642	0.123	0.960	0.086	0.675
0.0135	0.0344	498	277	901	501	2200	670	2.0	0.947	0.649	0.126	0.956	0.088	0.682
0.0137	0.0349	501	278	902	501	2196	669	2.0	0.945	0.654	0.128	0.954	0.089	0.687
0.0138	0.0352	501	278	902	501	2195	669	2.0	0.945	0.656	0.128	0.954	0.090	0.690
0.0140	0.0357	502	279	903	502	2196	669	2.0	0.945	0.661	0.130	0.954	0.091	0.695
0.0144	0.0367	503	279	905	503	2198	669	2.0	0.946	0.670	0.134	0.955	0.093	0.704
0.0146	0.0372	503	280	906	503	2200	670	2.0	0.947	0.674	0.136	0.956	0.095	0.709
0.0155	0.0395	501	279	910	506	2216	675	2.0	0.953	0.695	0.144	0.963	0.101	0.730
0.0170	0.0433	498	277	914	508	2236	681	2.0	0.962	0.716	0.158	0.972	0.110	0.752
0.0180	0.0458	496	276	916	509	2246	684	2.1	0.967	0.726	0.167	0.976	0.117	0.763
0.0190	0.0484	495	275	918	510	2254	686	2.1	0.970	0.735	0.177	0.980	0.123	0.772
0.0200	0.0509	495	275	920	511	2259	688	2.1	0.972	0.743	0.186	0.982	0.130	0.781
0.0210	0.0535	495	275	921	512	2263	689	2.1	0.974	0.750	0.195	0.983	0.136	0.789
0.0230	0.0585	496	275	923	513	2265	690	2.1	0.975	0.759	0.214	0.985	0.149	0.797
0.0280	0.0712	498	277	927	515	2270	691	2.1	0.977	0.779	0.260	0.987	0.181	0.818
0.0330	0.0839	499	277	930	517	2274	693	2.1	0.978	0.793	0.307	0.988	0.214	0.833
0.0830	0.2109	508	282	946	526	2294	699	2.1	0.987	0.875	0.770	0.997	0.537	0.920
0.1330	0.3379	514	286	958	532	2308	703	2.1	0.993	0.932	1.234	1.000	0.860	0.980
0.1830	0.4649	519	288	967	537	2318	706	2.1	0.998	0.977	1.698	1.000	1.184	1.000
0.2330	0.5919	522	290	971	540	2324	708	2.1	1.000	1.001	2.162	1.000	1.507	1.000
0.2830	0.7189	522	290	971	540	2324	708	2.1	1.000	1.000	2.625	1.000	1.830	1.000
0.3080	0.7824	522	290	971	540	2324	708	2.1	1.000	1.000	2.857	1.000	1.992	1.000

TABLE VI. - BOUNDARY LAYER SURVEY AT A NOMINAL MACH NUMBER OF 3.7 FOR COOLED INLET

[Free-stream velocity u_∞ = 2914 ft/sec (888 m/sec); wall temperature T_w = 633° R (352 K); free-stream stagnation temperature T_0 = 974° R (541 K); edge stagnation temperature $T_{t,e}$ = 964° R (536 K); velocity boundary layer thickness δ = 0.296 in. (0.752 cm); temperature boundary layer thickness Δ = 0.408 in. (1.036 cm).]

Integration to edge condition				Integration to free-stream condition			
Momentum, θ		Displacement, δ^*		Momentum, θ		Displacement, δ^*	
in.	cm	in.	cm	in.	cm	in.	cm
0.0073	0.0185	0.022	0.056	0.011	0.028	0.021	0.053

Distance from nozzle wall, y		Local static temperature, T		Local stagnation temperature, T_t		Local velocity, u		Local Mach number, M	Velocity ratio, u/u_∞	Temperature difference ratio, $\frac{T_t - T_w}{T_0 - T_w}$	Distance ratio, y/δ	Velocity, ratio, u/u_e	Distance ratio, y/Δ	Temperature difference ratio, $\frac{T_t - T_w}{T_{t,e} - T_w}$
in.	cm	°R	K	°R	K	ft/sec	m/sec							
0.0012	0.0032	607	337	761	423	1356	413	1.1	0.465	0.374	0.004	0.470	0.003	0.384
0.0042	0.0108	534	297	790	439	1755	534	1.5	0.602	0.460	0.014	0.608	0.010	0.474
0.0052	0.0133	505	280	799	444	1880	572	1.7	0.645	0.487	0.018	0.652	0.013	0.501
0.0062	0.0159	483	268	805	447	1968	599	1.8	0.675	0.505	0.021	0.682	0.015	0.520
0.0082	0.0210	461	256	815	453	2064	629	2.0	0.708	0.534	0.028	0.715	0.020	0.550
0.0102	0.0260	442	246	825	458	2144	653	2.1	0.736	0.562	0.035	0.743	0.025	0.579
0.0122	0.0311	431	239	834	463	2199	670	2.2	0.754	0.588	0.041	0.762	0.030	0.605
0.0162	0.0413	415	231	845	469	2272	692	2.3	0.780	0.621	0.055	0.787	0.040	0.639
0.0182	0.0464	407	226	849	472	2304	702	2.3	0.791	0.633	0.062	0.799	0.045	0.652
0.0212	0.0540	395	219	854	474	2349	716	2.4	0.806	0.648	0.072	0.814	0.052	0.667
0.0262	0.0667	374	208	863	479	2422	738	2.6	0.831	0.673	0.089	0.839	0.064	0.693
0.0313	0.0794	358	199	871	484	2482	756	2.7	0.852	0.697	0.106	0.860	0.077	0.717
0.0412	0.1048	327	182	886	492	2592	789	2.9	0.889	0.742	0.139	0.898	0.101	0.764
0.0462	0.1175	316	176	894	497	2634	802	3.0	0.904	0.764	0.156	0.913	0.113	0.787
0.0512	0.1302	305	169	901	500	2675	815	3.1	0.918	0.785	0.173	0.927	0.126	0.808
0.0542	0.1378	299	166	904	502	2696	821	3.2	0.925	0.795	0.183	0.935	0.133	0.818
0.0612	0.1556	288	160	912	507	2739	834	3.3	0.940	0.818	0.207	0.949	0.150	0.842
0.0702	0.1784	276	153	922	512	2785	848	3.4	0.956	0.847	0.237	0.965	0.172	0.872
0.0762	0.1937	269	150	926	514	2808	855	3.5	0.963	0.859	0.258	0.973	0.187	0.884
0.0812	0.2064	265	147	927	515	2821	859	3.5	0.968	0.863	0.275	0.978	0.199	0.888
0.0872	0.2216	260	145	929	516	2835	864	3.6	0.973	0.869	0.295	0.983	0.214	0.895
0.0912	0.2318	259	144	930	517	2841	865	3.6	0.975	0.872	0.308	0.985	0.224	0.898
0.0952	0.2419	257	143	931	517	2846	867	3.6	0.977	0.875	0.322	0.987	0.234	0.900
0.0982	0.2496	256	142	932	518	2849	868	3.6	0.978	0.876	0.332	0.987	0.241	0.902
0.1012	0.2572	256	142	933	518	2851	868	3.6	0.978	0.878	0.342	0.988	0.248	0.904
0.1112	0.2826	256	142	935	519	2855	870	3.6	0.980	0.885	0.376	0.989	0.273	0.911
0.1412	0.3588	257	143	938	521	2860	871	3.6	0.981	0.894	0.478	0.991	0.347	0.920
0.1712	0.4350	258	143	941	523	2865	873	3.6	0.983	0.905	0.579	0.993	0.420	0.931
0.2512	0.6382	261	145	951	528	2879	877	3.6	0.988	0.932	0.849	0.998	0.617	0.959
0.4712	1.1970	266	148	970	539	2908	886	3.6	0.998	0.988	1.593	1.000	1.156	1.000
0.6612	1.6796	267	148	974	541	2914	888	3.6	1.000	1.000	2.235	1.000	1.623	1.000

TABLE VII. - BOUNDARY LAYER SURVEY AT A NOMINAL MACH NUMBER OF 4.4 FOR COOLED INLET

[Free-stream velocity u_∞ = 3062 ft/sec (933 m/sec); wall temperature T_w = 572° R (318 K); free-stream stagnation temperature T_0 = 970° R (539 K); edge stagnation temperature $T_{t,e}$ = 961° R (534 K); velocity boundary layer thickness δ = 0.403 in. (1.024 cm); temperature boundary layer thickness Δ = 0.554 in. (1.407 cm).]

Integration to edge condition				Integration to free-stream condition			
Momentum, θ		Displacement, δ^*		Momentum, θ		Displacement, δ^*	
in.	cm	in.	cm	in.	cm	in.	cm
0.011	0.028	0.061	0.155	0.016	0.041	0.061	0.155

Distance from nozzle wall, y		Local static temperature, T		Local stagnation temperature, T_t		Local velocity, u		Local Mach number, M	Velocity ratio, u/u_∞	Temperature difference ratio, $\frac{T_t - T_w}{T_0 - T_w}$	Distance ratio, y/δ	Velocity, ratio, u/u_e	Distance ratio, y/Δ	Temperature difference ratio, $\frac{T_t - T_w}{T_{t,e} - T_w}$
in.	cm	°R	K	°R	K	ft/sec	m/sec							
0.0012	0.0032	629	350	721	400	1049	319	0.9	0.343	0.373	0.003	0.346	0.002	0.383
0.0042	0.0108	542	301	749	416	1576	480	1.4	0.515	0.445	0.011	0.520	0.008	0.456
0.0102	0.0260	476	264	788	438	1938	590	1.8	0.633	0.543	0.025	0.639	0.018	0.556
0.0142	0.0362	445	247	801	445	2066	629	2.0	0.675	0.574	0.035	0.682	0.026	0.588
0.0202	0.0514	419	233	813	452	2177	663	2.2	0.711	0.606	0.050	0.718	0.037	0.621
0.0362	0.0921	372	207	836	465	2360	719	2.5	0.771	0.664	0.090	0.779	0.065	0.680
0.0622	0.1581	308	171	866	481	2587	788	3.0	0.845	0.737	0.154	0.854	0.112	0.755
0.0842	0.2140	270	150	887	493	2723	829	3.4	0.889	0.790	0.209	0.898	0.152	0.810
0.1042	0.2648	241	134	904	502	2821	859	3.7	0.921	0.833	0.259	0.931	0.188	0.854
0.1242	0.3156	220	122	917	510	2894	882	4.0	0.945	0.866	0.308	0.955	0.224	0.888
0.1322	0.3359	212	118	922	512	2919	889	4.1	0.953	0.878	0.328	0.963	0.239	0.900
0.1422	0.3613	205	114	927	515	2944	897	4.2	0.962	0.890	0.353	0.971	0.257	0.912
0.1522	0.3867	199	111	930	517	2964	903	4.3	0.968	0.900	0.378	0.978	0.275	0.922
0.1602	0.4070	195	108	932	518	2977	907	4.4	0.972	0.904	0.398	0.982	0.289	0.927
0.1702	0.4324	190	106	934	519	2989	911	4.4	0.976	0.909	0.422	0.986	0.307	0.932
0.1762	0.4477	189	105	935	520	2995	912	4.4	0.978	0.912	0.437	0.988	0.318	0.935
0.1842	0.4680	186	104	936	520	3000	914	4.5	0.980	0.913	0.457	0.990	0.333	0.936
0.1942	0.4934	185	103	936	520	3005	915	4.5	0.981	0.915	0.482	0.991	0.351	0.937
0.1982	0.5036	184	102	937	520	3006	916	4.5	0.982	0.915	0.492	0.992	0.358	0.938
0.2042	0.5188	184	102	937	521	3007	916	4.5	0.982	0.916	0.507	0.992	0.369	0.939
0.2242	0.5696	184	102	938	521	3010	917	4.5	0.983	0.920	0.556	0.993	0.405	0.943
0.2442	0.6204	184	102	940	522	3013	918	4.5	0.984	0.923	0.606	0.994	0.441	0.946
0.2542	0.6458	184	102	941	523	3014	918	4.5	0.984	0.925	0.631	0.994	0.459	0.948
0.3142	0.7982	185	103	945	525	3022	920	4.5	0.987	0.937	0.780	0.997	0.567	0.960
0.3742	0.9506	186	103	949	527	3028	922	4.5	0.989	0.947	0.928	0.999	0.675	0.970
0.3982	1.0116	186	103	951	528	3030	923	4.5	0.990	0.951	0.988	1.000	0.719	0.974
0.4842	1.2300	187	104	957	532	3040	926	4.5	0.993	0.966	1.201	1.000	0.874	0.990
0.6343	1.6110	189	105	965	536	3053	930	4.5	0.997	0.987	1.573	1.000	1.145	1.000
0.7343	1.8650	190	105	969	538	3060	932	4.5	0.999	0.997	1.822	1.000	1.325	1.000
0.8642	2.1952	190	106	970	539	3062	933	4.5	1.000	1.000	2.144	1.000	1.560	1.000

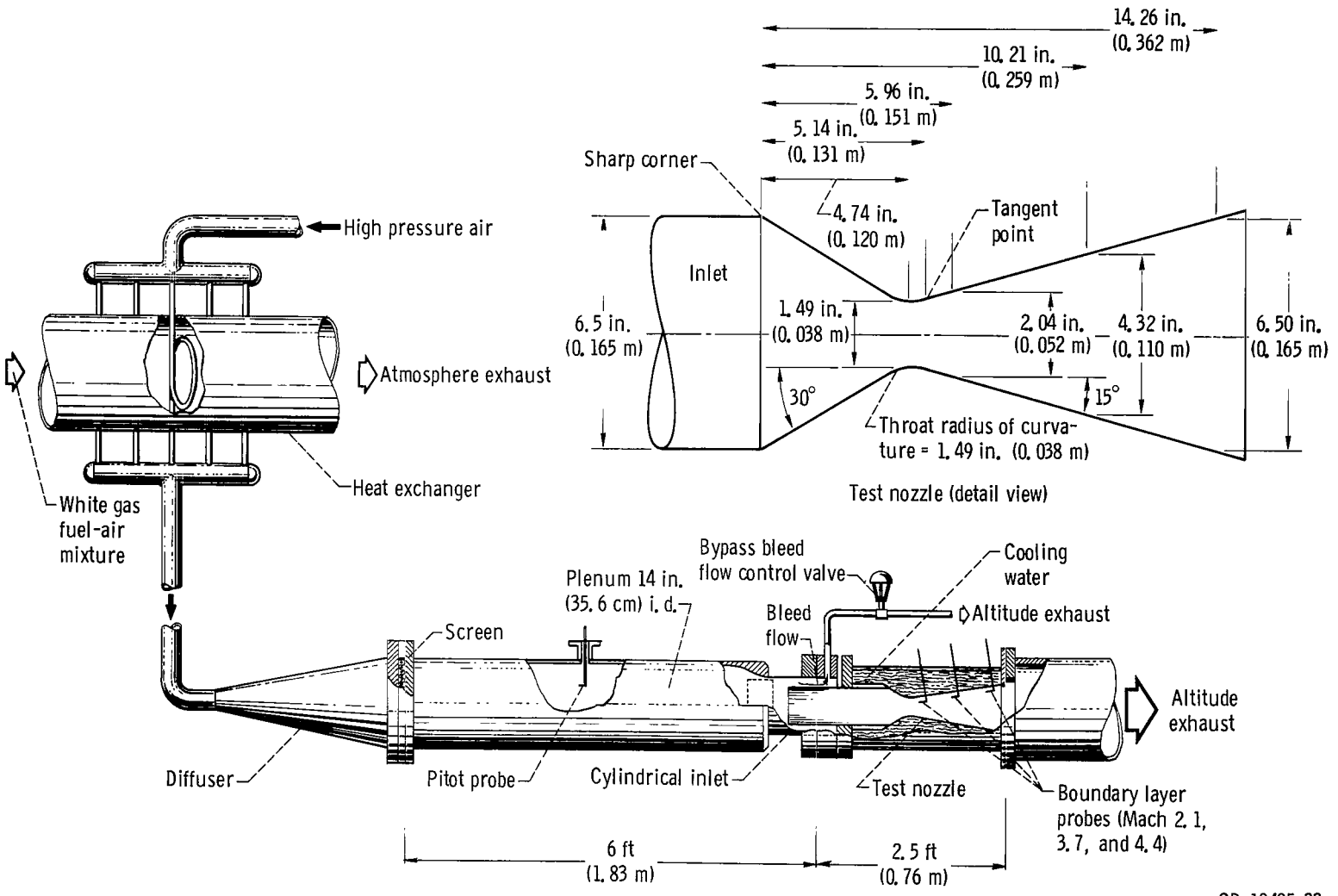

Figure 1. - Schematic diagram of nozzle heat transfer facility.

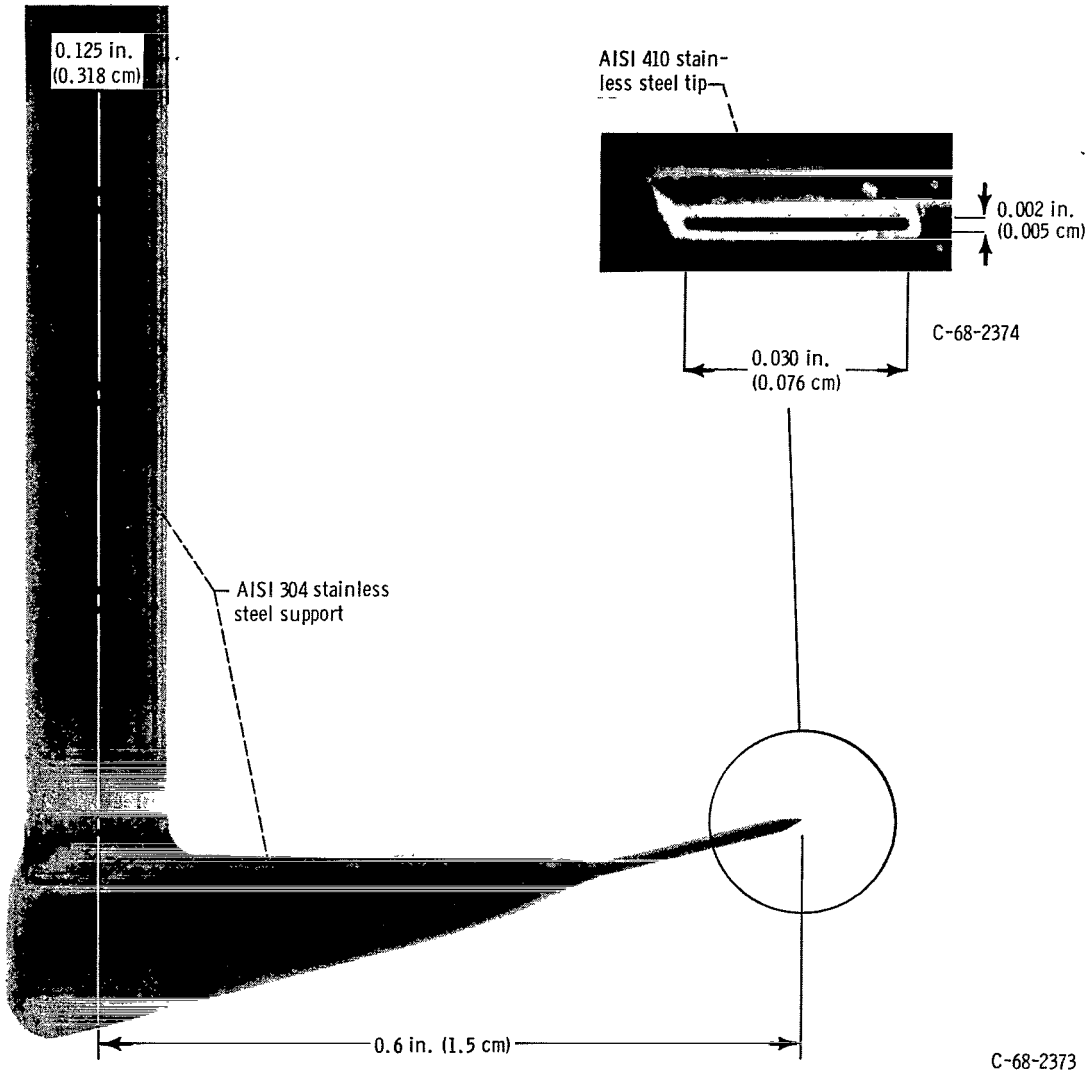

Figure 2. - Boundary layer pressure probe.

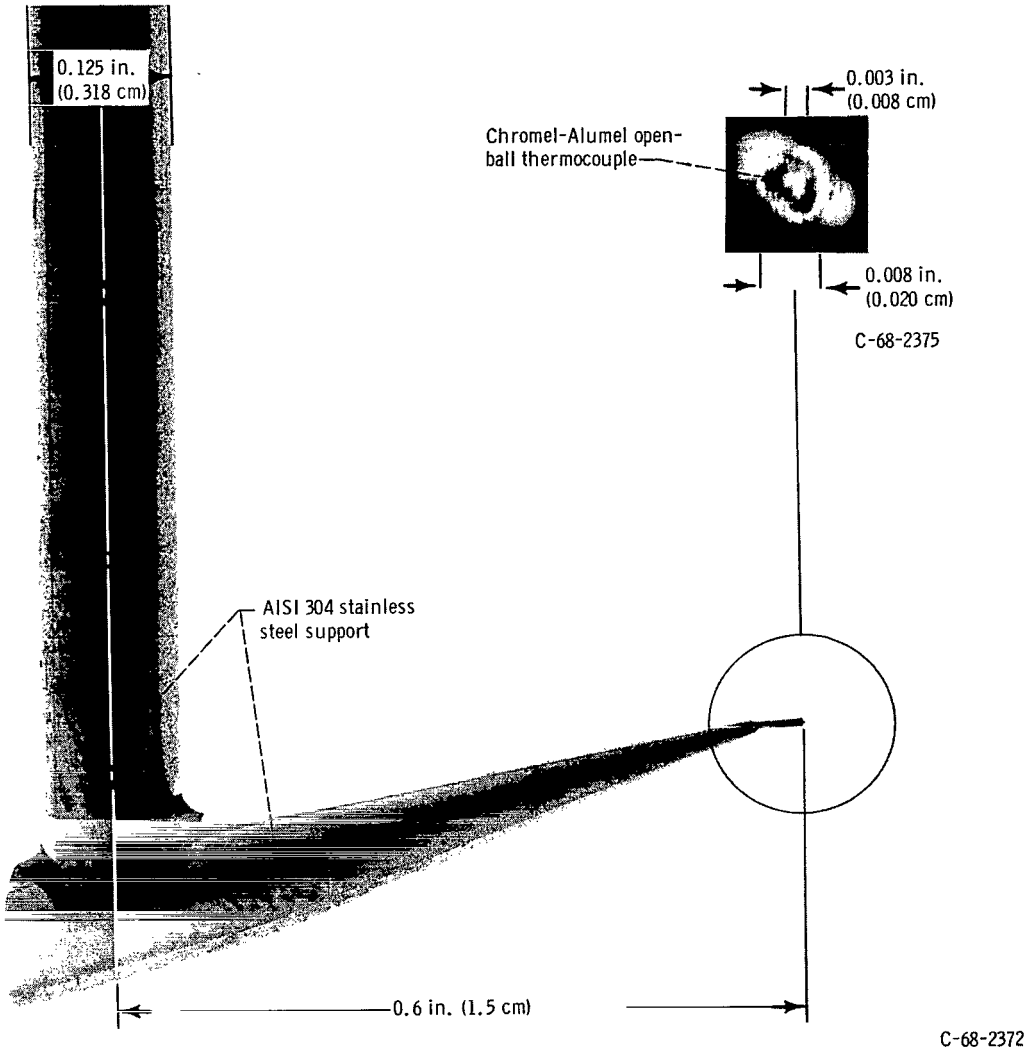

Figure 3. - Boundary layer temperature probe.

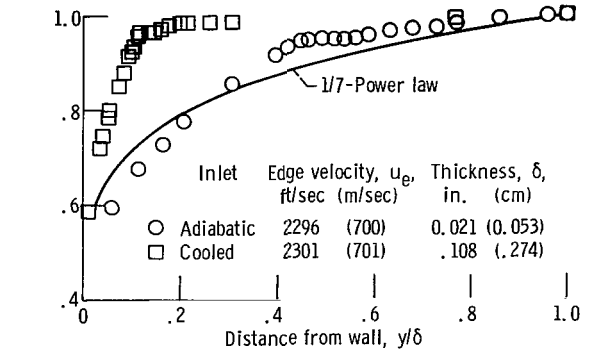

(a) Velocity ratio $u/u_e = f(y/\delta)$.

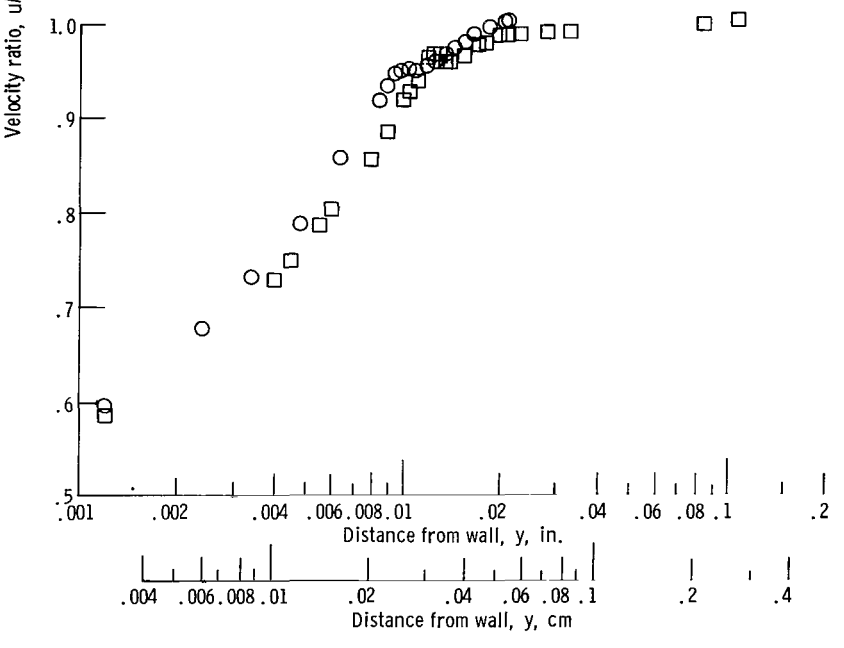

(b) Velocity ratio $u/u_e = f(y)$.

Figure 4. - Velocity profiles at free-stream Mach number of 2.1 corresponding to tests with adiabatic and cooled inlet (tables II and V, respectively). Stagnation temperature $T_0 \approx 970°$ R (539 K); stagnation pressure $P_0 \approx 300$ pounds per square inch (20.7×10^5 N/m^2) absolute.

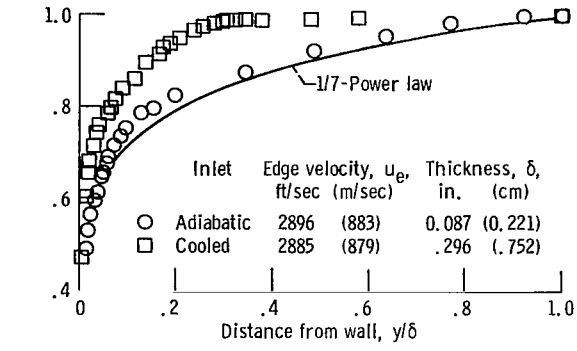

(a) Velocity ratio $u/u_e = f(y/\delta)$.

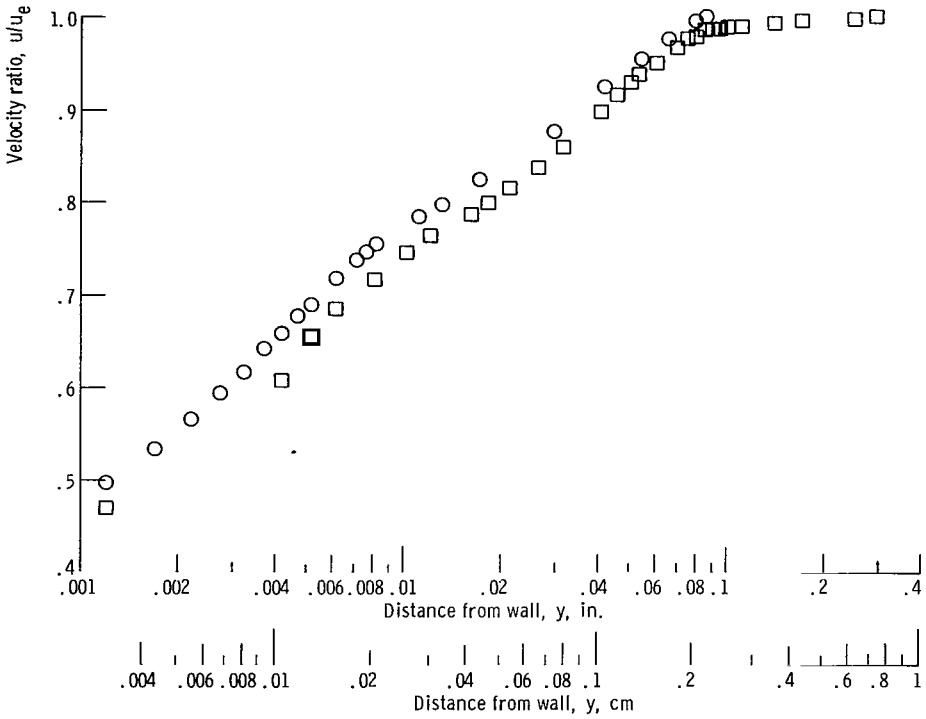

(b) Velocity ratio $u/u_e = f(y)$.

Figure 5. - Velocity profiles at free-stream Mach number of 3.7 corresponding to tests with adiabatic and cooled inlet (tables III and VI, respectively). Stagnation temperature $T_0 \approx 970°$ R (539 K); stagnation pressure $P_0 \approx 300$ pounds per square inch (20.7×10^5 N/m^2) absolute.

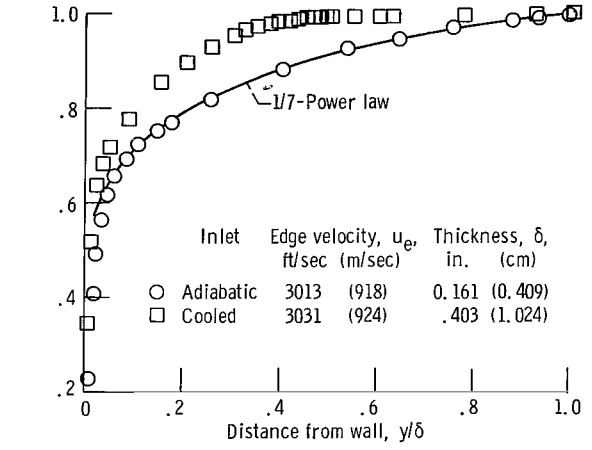

(a) Velocity ratio $u/u_e = f(y/\delta)$.

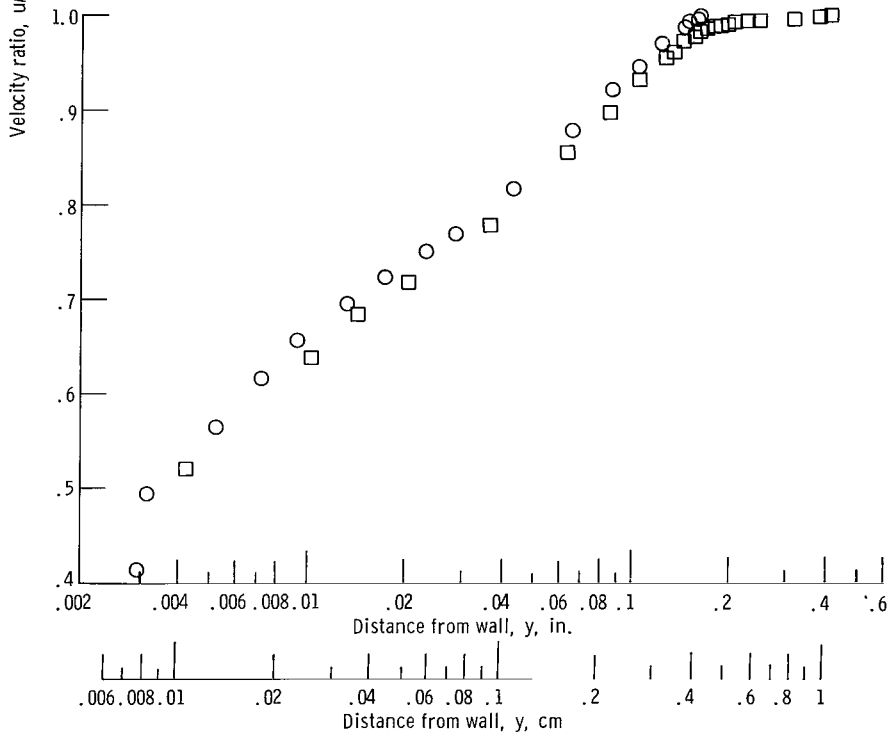

(b) Velocity ratio $u/u_e = f(y)$.

Figure 6. - Velocity profiles at free-stream Mach number of 4.4 corresponding to tests with adiabatic and cooled inlet (tables IV and VII, respectively). Stagnation temperature $T_0 \approx 970°$ R (539 K); stagnation pressure $P_0 \approx 300$ pounds per square inch (20.7×10^5 N/m^2) absolute.

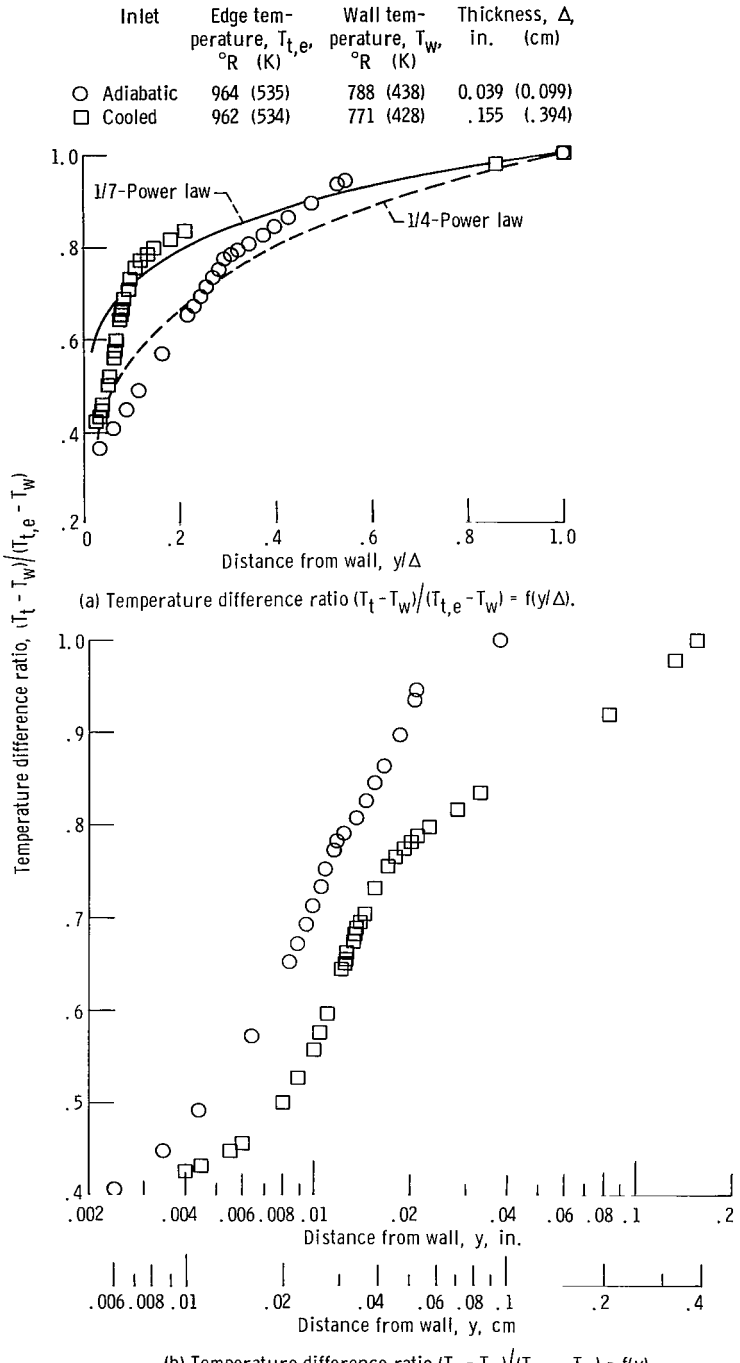

(a) Temperature difference ratio $(T_t - T_w)/(T_{t,e} - T_w) = f(y/\Delta)$.

(b) Temperature difference ratio $(T_t - T_w)/(T_{t,e} - T_w) = f(y)$.

Figure 8. - Temperature profiles at free-stream Mach number of 2.1 corresponding to tests with adiabatic and cooled inlet (tables II and V, respectively). Stagnation temperature $T_0 \approx 970°$ R (539 K); stagnation pressure $P_0 \approx 300$ pounds per square inch (20.7×10^5 N/m^2) absolute.

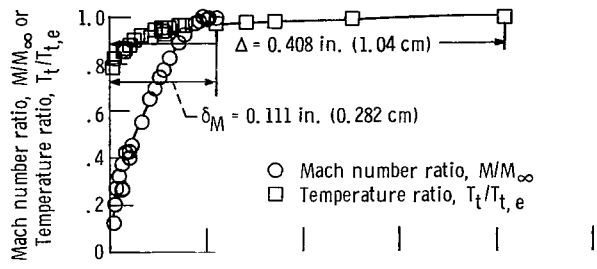

(a) Mach number and temperature profiles. Edge stagnation temperature $T_{t,e}$ = 964° R (536 K).

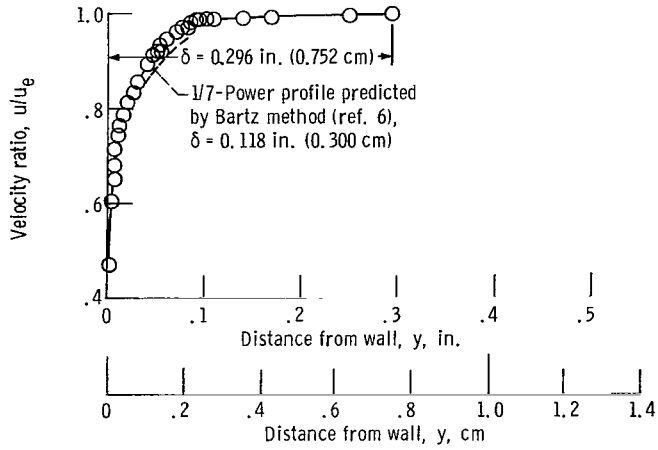

(b) Velocity profile. Edge velocity u_e = 2885 feet per second (879 m/sec).

Figure 7. - Mach number, temperature and velocity distributions at free-stream Mach number of 3.7 corresponding to tests with cooled inlet.

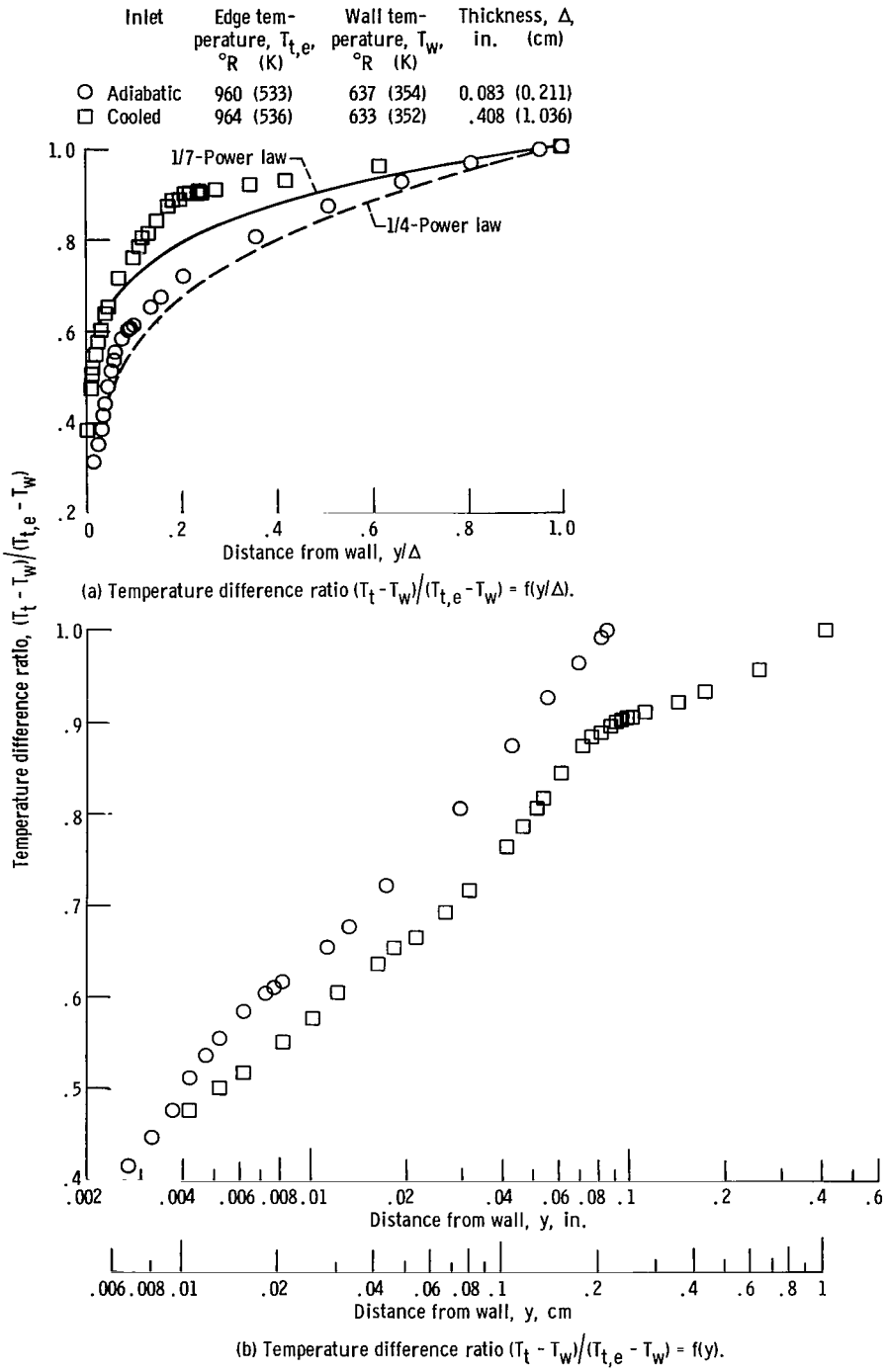

(a) Temperature difference ratio $(T_t - T_w)/(T_{t,e} - T_w) = f(y/\Delta)$.

(b) Temperature difference ratio $(T_t - T_w)/(T_{t,e} - T_w) = f(y)$.

Figure 9. - Temperature profiles at free-stream Mach number of 3.7 corresponding to tests with adiabatic and cooled inlet (tables III and VI, respectively). Stagnation temperature $T_0 \approx 970°$ R (539 K); stagnation pressure $P_0 \approx 300$ pounds per square inch (20.7×10^5 N/m^2) absolute.

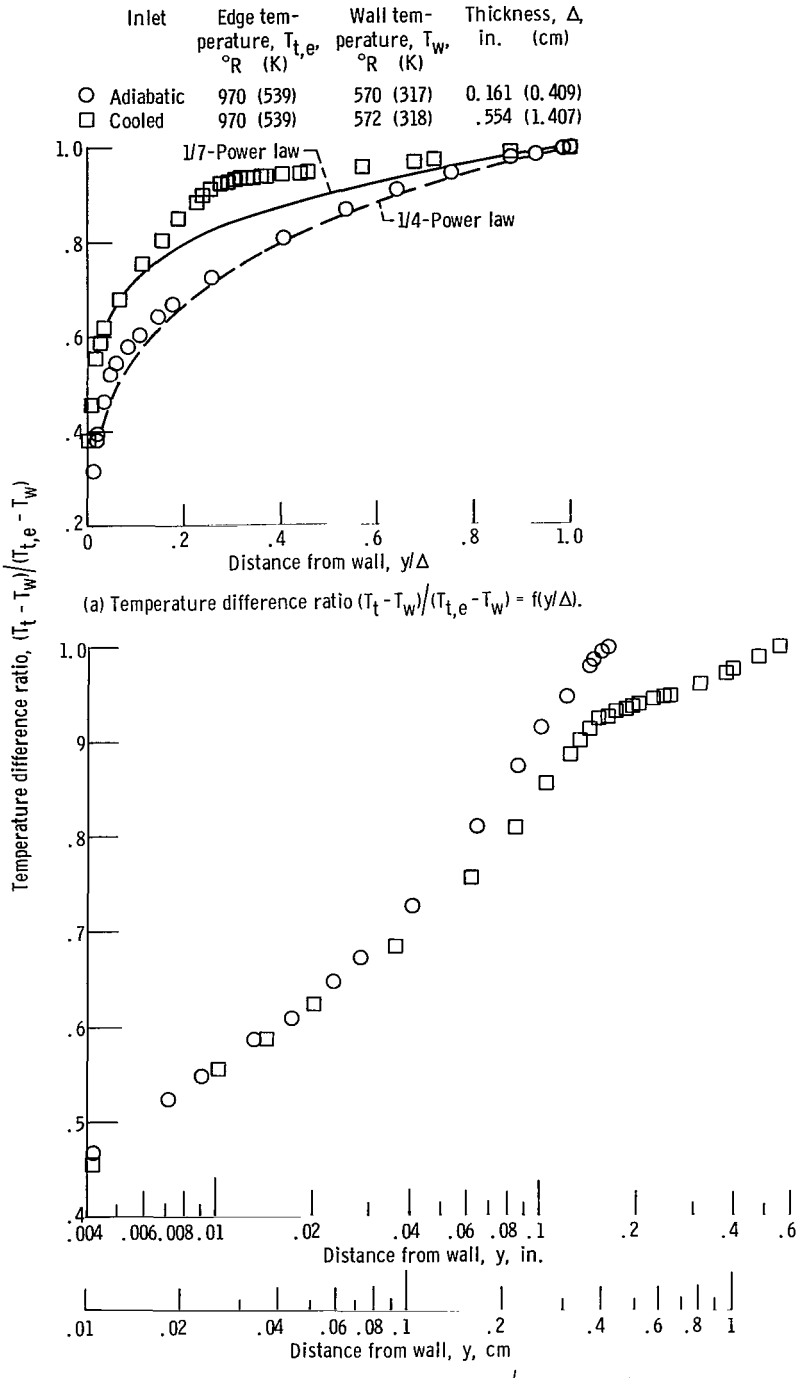

(a) Temperature difference ratio $(T_t - T_w)/(T_{t,e} - T_w) = f(y/\Delta)$.

(b) Temperature difference ratio $(T_t - T_w)/(T_{t,e} - T_w) = f(y)$.

Figure 10. - Temperature profiles at free-stream Mach number of 4.4 corresponding to tests with adiabatic and cooled inlet (tables IV and VII, respectively). Stagnation temperature $T_0 \approx 970°$ R (539 K); stagnation pressure $P_0 \approx 300$ pounds per square inch (20.7×10^5 N/m^2) absolute.

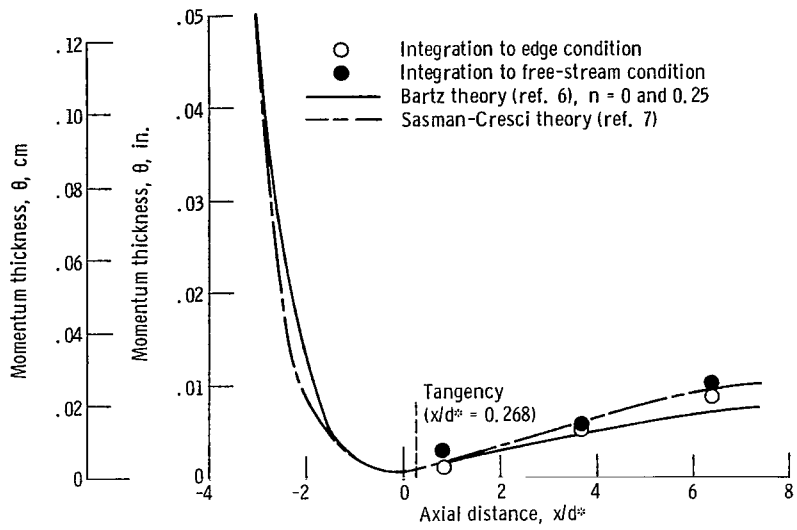

Figure 11. - Theoretical and experimental momentum thickness distributions corresponding to tests with adiabatic inlet. Throat diameter d* = 1.492 inches (3.790 cm).

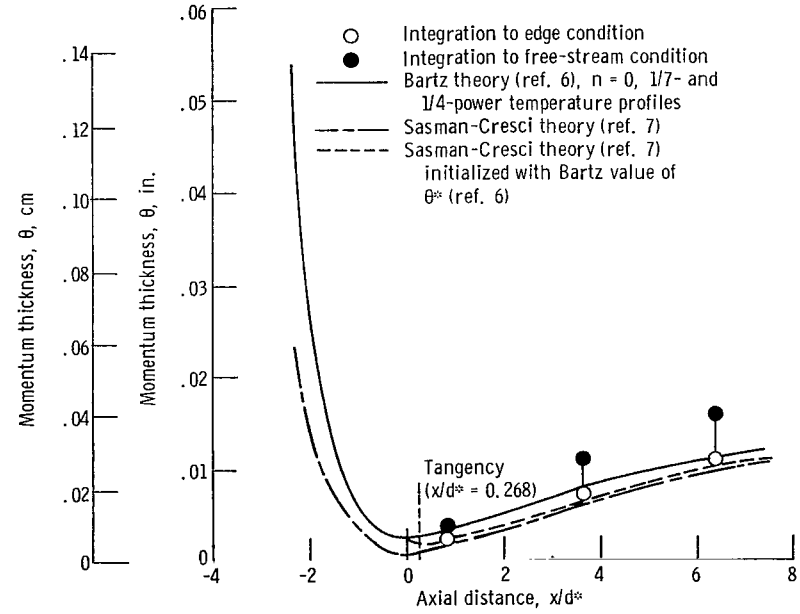

Figure 12. - Theoretical and experimental momentum thickness distributions corresponding to tests with cooled inlet. Throat diameter d* = 1.492 inches (3.790 cm).

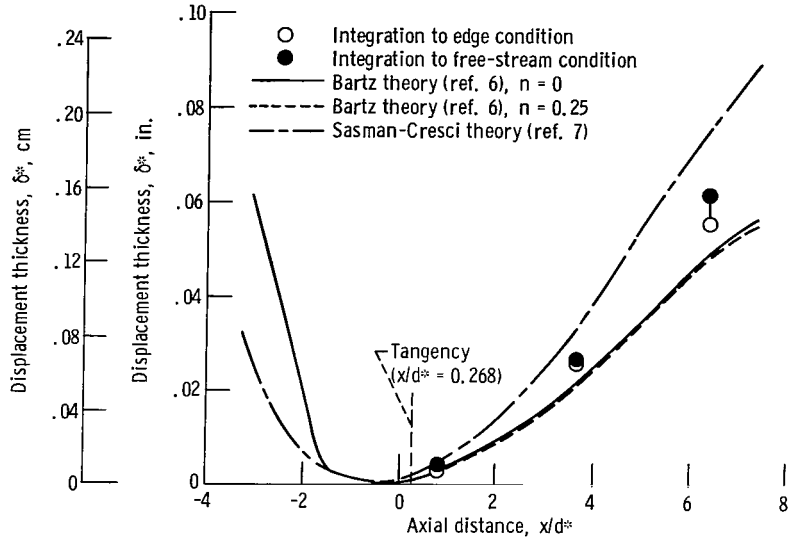

Figure 13. - Theoretical and experimental displacement thickness distributions corresponding to tests with adiabatic inlet. Throat diameter d^* = 1.492 inches (3.790 cm).

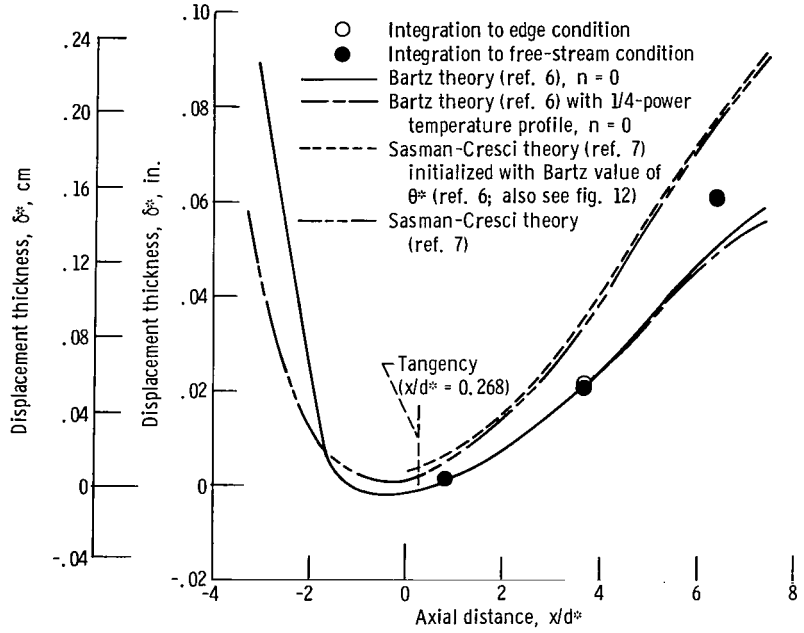

Figure 14. - Theoretical and experimental displacement thickness distributions corresponding to tests with cooled inlet. Throat diameter d^* = 1.492 inches (3.790 cm).

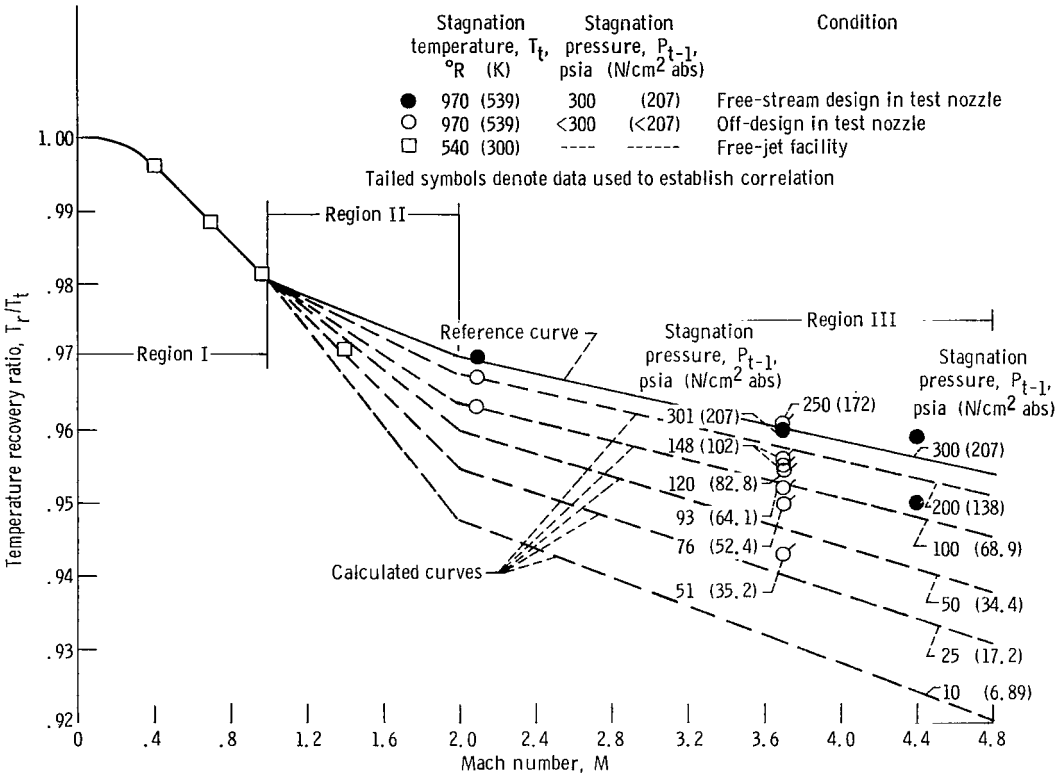

Figure 15. - Variation of recovery ratio with Mach number and stagnation pressure for boundary layer temperature probe.

NATIONAL AERONAUTICS AND SPACE ADMINISTRATION
WASHINGTON, D.C. 20546
OFFICIAL BUSINESS

FIRST CLASS MAIL

POSTAGE AND FEES PAID
NATIONAL AERONAUTICS AND
SPACE ADMINISTRATION

"The aeronautical and space activities of the United States shall be conducted so as to contribute . . . to the expansion of human knowledge of phenomena in the atmosphere and space. The Administration shall provide for the widest practicable and appropriate dissemination of information concerning its activities and the results thereof."

—NATIONAL AERONAUTICS AND SPACE ACT OF 1958

NASA SCIENTIFIC AND TECHNICAL PUBLICATIONS

TECHNICAL REPORTS: Scientific and technical information considered important, complete, and a lasting contribution to existing knowledge.

TECHNICAL NOTES: Information less broad in scope but nevertheless of importance as a contribution to existing knowledge.

TECHNICAL MEMORANDUMS: Information receiving limited distribution because of preliminary data, security classification, or other reasons.

CONTRACTOR REPORTS: Scientific and technical information generated under a NASA contract or grant and considered an important contribution to existing knowledge.

TECHNICAL TRANSLATIONS: Information published in a foreign language considered to merit NASA distribution in English.

SPECIAL PUBLICATIONS: Information derived from or of value to NASA activities. Publications include conference proceedings, monographs, data compilations, handbooks, sourcebooks, and special bibliographies.

TECHNOLOGY UTILIZATION PUBLICATIONS: Information on technology used by NASA that may be of particular interest in commercial and other non-aerospace applications. Publications include Tech Briefs, Technology Utilization Reports and Notes, and Technology Surveys.

Details on the availability of these publications may be obtained from:

SCIENTIFIC AND TECHNICAL INFORMATION DIVISION

NATIONAL AERONAUTICS AND SPACE ADMINISTRATION

Washington, D.C. 20546